Site-specific acetylation of polynucleotide kinase 3'-phosphatase (PNKP) regulates its distinct role in DNA repair pathways

Azharul Islam[1], Anirban Chakraborty[1], Altaf H Sarker[2], Uma K Aryal[3], Gulshan Sharma[1], Istvan Boldogh[4], Tapas Hazra[1*]

[1]Department of Internal Medicine, University of Texas Medical Branch, Galveston, TX, 77555, USA

[2]Life Sciences Division, Lawrence Berkeley National Laboratory, Berkeley, CA 94720, USA

[3]Purdue Proteomics Facility, Bindley Bioscience Center, Purdue University, IN 47907, USA

[4]Department of Microbiology and Immunology, University of Texas Medical Branch, Galveston, TX 77555, USA

*Address correspondence to

Tapas Hazra

Department of Internal Medicine-Pulmonary, Critical Care & Sleep Medicine

University of Texas Medical Branch, Galveston, TX 77555, USA

Tel: (409) 772-6308 Fax: (409) 747-8608

E-mail: tkhazra@utmb.edu

Abstract

Mammalian polynucleotide kinase 3'-phosphatase (PNKP) is a dual-function DNA end-processing enzyme with 3'-phosphatase and 5'-kinase activities, which generate 3'-OH and 5'-phosphate termini respectively, as substrates for DNA polymerase and DNA ligase to complete DNA repair. PNKP is thus involved in multiple DNA repair pathways, including base excision (BER), single-strand break (SSBR), and double-strand break repair (DSBR). However, little is known as to how PNKP functions in such diverse repair processes, involving distinct sets of proteins. Here, we report that PNKP is acetylated at two lysine (K142 and K226) residues. While K142 is constitutively acetylated by p300, CBP acetylates K226 only after DSB induction. Co-immunoprecipitation analysis involving antibodies specific for PNKP peptides containing AcK142 or AcK226 of PNKP showed that AcK142-PNKP associates only with BER/SSBR and AcK226 PNKP with DSBR proteins. Although acetylation at those residues did not significantly affect the enzymatic activity of PNKP *in vitro*, cells expressing non-acetylable PNKP (K142R or K226R) accumulated DNA damage, specifically in transcribed genes. Intriguingly, K142, but not K226, was acetylated in striatal neuronal cells of a Huntington's Disease (HD)-based mouse model. This is consistent with the reported degradation of CBP but not p300 in HD cells. Moreover, genomes of HD cells progressively accumulated DSBs specifically in the transcribed genes. Chromatin-immunoprecipitation analysis using anti-AcK142 or anti-AcK226 antibodies showed an association of Ac-PNKP with the transcribed genes, consistent with PNKP's role in transcription-coupled repair. Thus, our findings collectively demonstrate that acetylation at two lysine residues located in different domains of PNKP regulates its functionally distinct role in BER/SSBR vs. DSBR.

Introduction

Mammalian cells continuously incur a plethora of DNA damage, induced by various endogenous and exogenous genotoxic agents (1,2). Among myriad types of DNA lesions, of major threat to genomic integrity and species survival are DNA strand breaks, both single strand (SSBs) and double strand (DSBs), particularly in the transcribed region. Moreover, DNA strand breaks generated in a natural environment, or as DNA base excision repair (BER) intermediates, rarely harbor the canonical 3'-OH and 5'-phosphates. In most cases, these DNA ends are chemically modified and require further processing. 3'-phosphate (3'-P) is one of the major blocked DNA termini in mammalian cells and such DNA ends, in addition to impeding DNA repair, can stall elongating RNA polymerases (3). Thus, processing of the "non-ligatable" 3'-P-containing DNA termini is essential for repair progression and efficient transcription in mammalian cells. The 5'-OH DNA end is also another blocked DNA termini, generated during Okazaki DNA fragment processing and some endonuclease-mediated cleavage of genomic DNA (4). Polynucleotide kinase 3'-phosphatase (PNKP) is a bifunctional DNA end-processing enzyme for blocked DNA termini (3'-P and 5'-OH) at strand breaks in the mammalian genome (5-10). PNKP removes the 3'-P group and catalyzes the phosphorylation of the 5'-OH end to generate the canonical 3'-OH and 5'-P DNA termini, respectively, which is necessary for the subsequent activity of DNA polymerase in gap-filling, and DNA ligases in rejoining the two canonical DNA termini and completing the repair process.

Oxidized DNA bases are one of the major endogenous DNA lesions in mammalian cells and are primarily repaired via the BER pathway. We previously showed that the repair of oxidized DNA by two oxidized-base-specific DNA glycosylases, NEIL1 and NEIL2, predominantly produces 3'-P termini (11,12) which are efficiently processed by PNKP (11,13). We and the Mitra group subsequently established that NEIL1 and 2 preferentially repair the transcribed genome in mammalian cells via the transcription-coupled BER (TC-BER) pathway where PNKP plays a critical role (14,15). PNKP is the major DNA 3'-phosphatase in mammalian cells (7,16,17) and thus, it is also involved in the repair of SSBs via TC-SSBR. Moreover, several of our recent reports demonstrated a key role of PNKP in nascent RNA-templated error-free DSB repair of 3'P-containing termini in the transcribed genome via the transcription-coupled non-homologous end joining (TC-NHEJ) pathway in mammalian cells (17-19). Our studies further revealed that PNKP associates with transcription factors, RNAPII and other repair proteins to form distinct

pathway-specific pre-formed repair complexes (15,18,19). However, how PNKP coordinates such multistep and highly complex repair pathways involving distinct sets of proteins remains mostly elusive.

Post-translational modifications of proteins play important roles in diverse cellular processes, including association with other proteins. Phosphorylation of PNKP by Ataxia telangiectasia mutated (ATM) and DNA-dependent protein kinase (DNA-PK) has been reported and was shown to stabilize the protein and modestly enhance PNKP's activity (20,21). To investigate whether an additional modification in PNKP takes place and plays any role in determining pathway choice, mass spectrometry (MS) analysis of FLAG-tagged PNKP (affinity purified from mammalian cells) was performed. PNKP was found to undergo acetylation at two sites: constitutively in one site at K142, and a second site at K226, only after the cells were treated with the radiomimetic drug, Bleomycin (DSB inducing agent; Bleo). Of note, unlike other DNA repair proteins, recombinant PNKP, purified from *E. coli*, was found to be acetylated at multiple sites for unknown reasons. We subsequently generated stably expressing individual K142R, K226R, and K142/K226R mutant cell lines, purified both WT and the mutant proteins from the corresponding cells (±Bleo), and further confirmed by MS analysis that K142 and K226 are indeed the major acetylation sites in PNKP. Finally, we showed that two different acetyl transferases, p300 and CREB-binding protein (CBP), acetylate the two lysines, K142 and K226, respectively, and provided evidence supporting how such distinct site-specific acetylation plays a vital role of PNKP in TC-BER/SSBR vs. TC-NHEJ pathways in mammalian cells.

Materials and Methods:

Cell culture and treatment conditions

Human embryonic kidney (HEK293) cells and HEK293-derived stable cell lines expressing FLAG-tagged WT and mutant (K142R, K226R, K142R/K2226R, K142Q, K226Q and K142Q/K226Q) PNKP protein were cultured and maintained in DMEM:F12 (1:1) (Cellgro) containing 10% fetal bovine serum (R & D Systems-Biotechne), 100 units/ml penicillin, streptomycin and amphotericin B (ThermoFisher Scientific) in a 5% CO_2 incubator at 37 °C with 95% relative humidity. Mouse striatal neuronal cells, Q7 and Q111 (striatal derived cell line from a knock in transgenic mouse containing homozygous Huntingtin (HTT) loci with a humanized Exon 1 containing 7 or 111 polyglutamine repeats, respectively), were cultured and

maintained in Dulbecco Modified Eagles Medium (high glucose) with 2mM L-glutamine containing 10% fetal bovine serum, 100 units/ml penicillin and streptomycin, and 0.4 mg/ml G418. While culturing these cells, repeated or high number of cell passages were avoided. All the cell lines (initial source: ATCC for HEK293 cells and Corriell Institute for the Q7/Q111 cells; Cat# CH00097 and CH00095, respectively) were authenticated by Short Tandem Repeat (STR) analysis in the UTMB Molecular Genomics Core. We routinely tested for mycoplasma contamination in cultured cells using the Mycoalert Mycoplasma Detection Kit (Lonza) according to the manufacturer's protocol, and the cells were found to be free from mycoplasma contamination. WT and mutant (K/R and K/Q) PNKP expressing stable cell lines were transfected with 10 μM PNKP 3'-UTR specific siRNA for 48 h followed by treatment with Glucose oxidase (GO) (400 ng/ml) for 30 min or Bleomycin (Bleo) (30 μg/ml) for 1 h when cells reached approximately 70% confluency. Likewise, Q7 and Q111 cells were also treated with the same concentrations of GO or Bleo under the same experimental conditions.

Antibodies and Western blotting (WB)

The list of antibodies (Abs) used in this study and their sources are listed in **Table 1** WB analysis was performed following the protocol as described earlier (17,19,22,23). The10 dilution of all primary Abs used was 1:500, with the exception of GAPDH which was 1:7,000. The dilutions of the secondary HRP-conjugated anti-rabbit and anti-mouse IgG were 1:5,000 and 1:2,000, respectively. All Abs were diluted in 5% skim milk.

Generation of PNKP expressing stable cell lines

For generating the WT and mutant PNKP expressing stable cell lines, human embryonic kidney (HEK293) cells were transfected with PNKP-FLAG (WT and mutants) expressing vector (pcDNA3) in 6-well plates using Lipofectamine 2000 (ThermoFisher Scientific) according to the manufacturer's protocol. Stably expressing cells were selected with 400 mM geneticin (Millipore-Sigma) starting 48 h post-transfection, when the plasmid starts integrating into the genomic DNA, and continued until the surviving cells formed colonies. The individual colony was further allowed to grow in each 9.6 cm^2 dish with 100 mM geneticin until the cells reached 100% confluency. Finally, WT and mutant PNKP expressing stable cell lines were screened by immunoblotting with anti-FLAG M2 Ab and categorized as low, medium, or high expression cell lines as per the ectopic expression level of PNKP. All other necessary steps were performed

as mentioned earlier (22), and as described by the PCDNA3.1 user manual (Thermofisher Scientific).

Site-directed mutagenesis

The coding DNA sequence (CDS) of the human PNKP (gene accession#NM_007254.4) was amplified by the Q5 hot start high fidelity DNA polymerase (New England Biolabs) using HEK293 genomic DNA as a template, and the amplified PCR fragment was cloned in pCDNA3 (having N-terminal FLAG tag in it) using *Hin*dIII- *Bam*HI sites as described earlier (17). K142 and K226 were mutated to Arginine (K142R & K226R) or glutamine (K142Q & K226Q), individually, using the Q5 site-directed mutagenesis kit (New England Biolabs), according to the manufacturer's protocol. PCR primers for site-directed mutagenesis were designed using NEBaseChanger for generating mutations. The primers to introduce these mutations are listed in **Table 2**. A double mutant (K142R/K226R) was generated using the single mutant K142R as a template and introducing the K226R mutation in it. Similarly, a K142Q/K226Q double mutant was generated using K142Q as a template.

Cell fractionations and immunoprecipitation (IP)

FLAG-tagged WT and mutant cell lines were treated with GO or Bleo as described above. Cytoplasmic, nuclear, and chromatin cell fractions were prepared from these cells following the previously described protocol (17,24), with modifications as follows. Dithiothreitol (DTT) was excluded from the cytosolic, nuclear and chromatin fractionation buffers due to interference of DTT with the binding of FLAG-PNKP with Anti-FLAG M2 Affinity gel, a mouse monoclonal Ab that is covalently attached to agarose (Millipore Sigma). Moreover, 0.30 units/µL of benzonase (MilliporeSigma) was added to the chromatin fractionation buffer followed by incubation at 37 ^{o}C for 45 min. For immunoprecipitation, 30 µl of Anti-FLAG M2 Affinity gel was mixed with an appropriate volume of chromatin fraction containing 1 mg of total protein, and incubated in a rotatory shaker overnight at 4 °C. The immune complex was washed 3 times with wash buffer (20 mM HEPES, pH 7.9, 0.5 mM EDTA, 10% glycerol, 0.25% Triton X-100, 250 mM KCl, complete mini EDTA free protease inhibitor cocktail, Millipore Sigma), and FLAG-PNKP was eluted from the affinity gel using elution buffer (20 mM Tris HCl, pH 7.5, 150 mM NaCl, 10% glycerol, protease inhibitor cocktail) containing 150 mM FLAG peptide (Millipore Sigma). 20 µL of the eluted product was separated on SDS-PAGE and stained with

CBB followed by destaining, and the concentration of PNKP protein was determined using known standards of BSA. The resulting purified PNKP was used for downstream processes. The concentration of eluted WT and mutant FLAG-PNKP protein was further confirmed by densitometric analyses of immuboblot compared with the affinity-purified recombinant His-PNKP, using 3 μL eluted PNKP for SDS-PAGE separation (17,23). AcK142 PNKP was immunoprecipitated using 10 μg of custom-made rabbit polyclonal anti-AcK142 Ab (Ez Biolabs) from 1 mg of GO-treated chromatin fraction from WT-PNKP-FLAG and K142R-PNKP-FLAG expressing cells. Similarly, immunopulldown was performed from chromatin fraction of mock vs. Bleo-treated WT-PNKP-FLAG and K226R-PNKP-FLAG cell lines using 10 μg of custom-made rabbit polyclonal anti-AcK226 Abs (Ez Biolabs). All other subsequent steps and buffers used for IP were the same as described earlier (17,18). Immunocomplexes of both GO and Bleo-treated samples were probed with anti-FLAG Abs to detect AcK142 and AcK226 PNKP in the respective samples. Further, Co-IP experiments were performed in mock/GO and mock/Bleo-treated WT-PNKP-FLAG expressing cell lines to investigate if SSB and DSB repair proteins interact with the AcK142 and AcK226 PNKP, respectively. GO and Bleo treatment followed by Co-IP from the chromatin fraction was performed as described earlier with little modification. The immunocomplexes were tested for the presence of different SSB and DSB repair proteins using appropriate Abs.

Mass spectrometry analysis by LC-MS/MS

Mass spectrometry analysis by LC-MS/MS was performed at the Taplin Biological Spectrometry facility at Harvard Medical School. Immunoprecipitation (IP) of PNKP was performed as described in the *Cell Fractionations and IP* section. 30 μL immunoprecipitated (IP'd) WT and mutant (K226R) PNKP were separated by SDS-PAGE and gel bands of PNKP were excised after CBB staining. Following destaining, excised gel bands were cut into approximately 1 mm^3 pieces. Gel pieces were subjected to a modified in-gel trypsin digestion procedure (25) and the sample was run over a nanoscale processed reverse-phase HPLC capillary column (26). Eluted peptides were subjected to electrospray ionization and then entered into an LTQ Orbitrap Velos Pro ion-trap mass spectrometer (Thermo Fisher Scientific). Peptide sequences (and hence protein identity) were determined by matching protein or translated nucleotide databases with the acquired fragmentation pattern by the software program, Sequest (Thermo Finnigan) (27). The

differential modification of 42.0106 mass units to lysine was included in the database searches to determine acetylated peptides. All databases include a reversed version of all sequences, and the data were filtered to a 1-2% peptide false discovery rate.

Microscopic imaging

WT and mutant (K/R) PNKP expressing stable cell lines were transfected with the PNKP 3'-UTR specific siRNA as described above. Cells were then trypsinized and $1x10^5$ cells were plated on collagen pre-treated cover glasses (Roche Applied Sciences) followed by treatment with GO or Bleo. Likewise, Q7 and Q111 cells were also treated with GO or Bleo. Cells were then fixed with an acetone-methanol (1:1) solvent for 10 min at room temperature, and dried. Next, cells were rinsed and permeabilized using 0.1% (w/v) Tween-20 diluted in phosphate-buffered saline (PBST) for 5 min, incubated with 1% BSA for 1 h at room temperature, and then blocked with anti-mouse IgG (1:100 dilution) for 1 h at 37 ^{o}C. Mouse WT (Q7) and Huntington's Disease (HD)-derived striatal neuronal cells (Q111) were treated with 1% Triton X-100 for 15 min at room temperature, instead of Tween-20, for permeabilization. Cells were incubated with custom-generated anti-AcK142 and anti-AcK226 Abs (EZ BioLabs) at a dilution of 1:200 in PBST for 1 h at 37 □C. After 3 washes in PBST, the cells were incubated with a secondary Ab conjugated to Alexa Fluor 594 (goat anti-rabbit) for 1 h at 37 □C. After washing in PBST (3 times), cells were dried and mounted with Vecta shield/DAPI, 4′6-diamidino-2-phenylindole hydrochloride (Vector Laboratories). More than 20 randomly selected fields of view per sample were photographed using a WHN10×/22 eyepiece and a 60× objective (field of view is 1.1 mm, and camera correction is 1.0) on an Echo Revolution Microscope system.

***In vitro* 3'-phosphatase and 5'-kinase assays of PNKP**

The phosphatase activity of IP'd PNKP from mock vs. Bleo-treated WT, K142R, K226R, and K142R/K226R cells was determined by the *in vitro* 3'-phosphatase assay as described earlier (13,16,18,22) with little modification. 1 ng of IP'd WT and mutant PNKP and 7.5 pmole cold substrates were incubated with γP^{32} ATP radiolabeled 3'-phosphate-containing substrate (5 pmol) for 13 min at 37 ^{o}C in phosphatase assay buffer (25 mM Tris-HCl pH 7.5, 100 mM NaCl, 5 mM $MgCl_2$, 1 mM DTT, 10% glycerol, and 0.1 μg/μL acetylated BSA). Additionally, the 5'-kinase assay of above mentioned IP'd WT vs. mutant PNKP was performed as described earlier (28,29) with little modification. γP^{32} labeled ATP was incubated in kinase assay buffer (800 mM succinic acid pH 7.5, 100 mM $MgCl_2$, 10 mM DTT, 2.5% glycerol) along with 1.0 μg/μl

acetylated BSA, and 0.6 pmole labeled substrate for 30 min at 30 ^{o}C. 100 fmol of PNKP and 2.5 pmol cold substrate were used in this assay. For both the 3'-phosphatase and the 5'-kinase assays, the radioactive bands were visualized in PhosphorImager (GE Healthcare) and quantitated using ImageQuant software. The data were represented as % product released from the radiolabeled substrate.

Long amplicon quantitative PCR (LA-qPCR)

WT and mutant PNKP expressing stable cell lines were transfected with 10 μM PNKP-3'UTR specific siRNA (Horizon Discovery) in a 24-well plate using RNAiMAX (ThermoFisher Scientific) according to the manufacturer's protocol for the depletion of endogenous PNKP along with scrambled siRNA control for each. The sequences of PNKP's 3'UTR specific siRNA were as follows: sense sequence: CCU CCA CAA UAA ACG CUG U UU, and antisense sequence: ACA GCG UUU AUU GUG GAG G UU. 48 h post-transfection with siRNA, cells were either mock-treated or treated individually with Bleo or GO, and the cells were harvested at 16 h post-treatment for Bleo and 4 h post-treatment for GO. Harvested cells were used for two different biochemical analyses as follows: (a) Depletion of endogenous PNKP by siRNA. Total RNA was extracted from the Bleo/GO-treated and untreated (control) cells using TRIzol (ThermoFisher Scientific) according to the manufacturer's protocol. 1 μg of total RNA was used to make cDNA libraries using prime script RT reagent kit gDNA eraser (Takara Bio Inc.) according to the kit's protocol, and RT-PCR was carried out using 1 μl of cDNA to amplify the 3'UTR region of the endogenous PNKP gene, as well as the housekeeping gene (GAPDH) using quick-load Taq 2x master mix (New England Biolabs) according to manufacturer's protocol. The primers used for amplifying the 3'UTR region of PNKP and GAPDH are listed in **Table 2**. The amplified PCR products were run in 1.5% agarose gel and stained with ethidium bromide, and the image was processed by Gel Doc EZ imager (BioRad). The quantitation of gel bands was performed using ImageJ software and the endogenous PNKP expression was normalized using GAPDH. The relative expression levels were presented with the expression of endogenous PNKP in control siRNA transfected cells considered as 100. (b) Extraction of genomic DNA was performed using the QiaAmp DNA Micro kit (Qiagen) according to the manufacturer's protocol, and the concentration was determined by the NanoVue (GE Healthcare). Gene-specific LA-qPCR assays for measuring DNA strand-breaks (SBs) were performed as described earlier (7,17,18,22) using Long Amp Taq DNA Polymerase (New England BioLabs). 10 ng of genomic DNA was used as

a template to amplify transcribed (10.4 kb region of the hypoxanthine-guanine phosphoribosyltransferase [HPRT], 12.2 kb of the DNA polymerase beta [POLB], 11.3 kb of the RNA polymerase II) and non-transcribed (8.6 kb of the Nanog homeobox [NANOG], 10.1 kb of the POU class 5 homeobox 1 [OCT 4] and 6.0 kb of the myosin heavy polypeptide 2, [MYH2]) genes, using the primers described previously (**Table 2**)(7,17,18). A similar set of LA-qPCR was performed in Q7 and Q111 cells following the same experimental procedures mentioned above without any GO/Bleo treatment. Since these are neuronal cells, a different set of transcribed ((neuronal differentiation factor 1 (NeuroD), tubulin β3 class III (TUBB) and POLB) vs. non-transcribed (myogenic differentiation factor [MyoD], muscle-specific myosin heavy chain 4 and 6 [MyH4, MyH6]) genes were used for the LA-qPCR assay. Since a short region would have less probability of DNA SBs, a short DNA fragment (short amplicon PCR; SA-PCR) from the same gene was also amplified for normalization of the amplified long fragment. To overcome the variation in PCR amplification while preparing the PCR reaction mixture, the LA-qPCR and SA-PCR reactions were set for all genes from the same stock of diluted genomic DNA samples. The amplified products were separated in 0.8% agarose gel and then stained with ethidium bromide followed by capturing the image by Gel Doc EZ imager (BioRad). The band intensity was determined by ImageJ software and the extent of DNA damage was calculated based on the relative quantification of the ratio of the large fragment and short fragment.

Detection of R-loop by Slot Blot assay

WT, K142R and K226R PNKP expressing stable cell lines were grown in a 24-well plate and depletion of endogenous PNKP was performed using 3’ UTR specific siRNA. Cells were individually treated in each well with Bleo at 48 h post-transfection of siRNA and harvested at 16 h post-treatment with Bleo. Genomic DNA was purified using DNeasy Blood and Tissue kit (Qiagen Cat# 69504) following the manufacturer's protocol. A restriction enzyme cocktail (*Eco*RI, *Hin*dIII, *Bsr*GI, and *Xba*I from NEB) was used to digest the nucleic acid overnight at 37 ^{o}C. Subsequently, DNA concentration was measured, and half of the digested DNA was incubated at 37 ^{o}C overnight with RNase H (Thermofisher) at a concentration of 5 units per 10 µg DNA. Slot blot was performed following the protocol described earlier (19). Genomic DNA from mock-treated (C), Bleo-treated (B) and 16 h post-Bleo-treated (R) cells, with or without RNase H digestion, were blotted (0.25 µg) onto high bond positively charged nylon membrane (Cytiva Amersham Cat# RPN12108) in duplicate. DNA was cross-linked using UV (Strata linker

1800) with an auto cross-link program and the membrane was blocked with 5% skim milk in PBST for 1 h. One membrane was probed with RNA-DNA (S9.6) hybrid Ab (Kerafast Cat# ENH001) at a dilution of 1:1000 overnight. The other membrane was incubated with an anti-dsDNA Ab (Abcam Cat# ab215896) (as a loading control) at a dilution of 1:2000 . After the incubation, the membranes were washed and incubated with the secondary Ab (goat anti-mouse HRP conjugated, Cell Signaling Technology) for 1 h, and nucleic acids were detected by super signal west pico (Thermo) or ECL select (Cytiva) and imaged with Varsadoc (BioRad) and quantified.

Lactate dehydrogenase (LDH) cytotoxicity assay

Cells expressing WT, K142R, K226R and K226R PNKP were counted after trypsinization, and $1x10^4$ cells were plated in a 24-well plate. Cells were transfected with 3' UTR specific siRNA for depletion of endogenous PNKP. Cells were individually treated with Bleo for 1 h in each well at 48 h post-transfection of siRNA. Subsequently, LDH cytotoxicity was performed according to the manufacturer's protocol (BioLegend, cat#426401). The output of triplicate samples was determined immediately at OD 450 nm on a microplate reader (Synergy H1 Hybrid Multi-Mode Reader; BioTek) at 37 °C under light-protected conditions. The amount of released LDH in media due to the induction of DNA double-strand break by Bleo was determined using the formula ΔA450 nm = (A2 – A1), where: A1 is the sample reading at 0 h and A2 is the sample reading at 2 h. DMEM without phenol red was used as a background control in this assay. LDH activity was expressed as nmoles of NADH generated by LDH reaction during the reaction time (ΔT = T2 – T1). LDH activity = (BI (ΔTx V)) × D = nmol/min/mL, where B = amount of NADH in the sample, calculated from a standard curve (nmol); ΔT = Reaction time (minutes); V = Original sample volume added into the reaction well (mL); and D = Sample dilution factor.

Chromatin immunoprecipitation (ChIP) assay:

ChIP assays were performed essentially as described earlier (17,30) with little modifications. Mock, GO or Bleo-treated WT-PNKP FLAG cells were incubated with 1% formaldehyde for 15 min at room temperature for cross-linking. Subsequently, the genomic DNA was fragmented to a size range of 300-500 bp by sonication (3-5 pulses of 30 seconds at 30 amplitude) using a sonicator (Qsonica-Q700). Total protein concentration was determined by a Bradford protein assay, and 100-500 μg of protein lysate was used for each IP. 10 μg of ChIP-grade, custom-made

rabbit polyclonal anti-AcK142- and anti-AcK226 (Ez Biolabs) Abs were incubated overnight at 4 °C with the lysate from mock vs. GO-treated or mock vs. Bleo-treated cells, respectively. Ab-protein-DNA complexes were captured by protein A-G agarose beads (SantaCruz Biotechnology) for 4 h at 4 °C. Buffers used and all subsequent steps including the elution of the immune complex, de-crosslinking, digestion of proteins and purification of the DNA were performed following the procedures as described earlier (17,30). The purified DNA was subjected to qPCR using CDS-specific primers (transcribed and non-transcribed gene-specific) as listed in **Table 2**.

Statistical analysis

A two-sided unpaired Student's *t*-test (http://www.ruf.rice.edu/~bioslabs/tools/stats/ttest.html) was used for the analysis of statistical significance between two sets and among three sets of data. The level of significance was evaluated at levels $P>0.05$ (ns), $P<0.05$ (*), $P<0.01$ (**) and $P<0.005$ or 0.0001 (***), as the case may be.

Results

Residues K142 and K226 are acetylated in human PNKP

The role of phosphorylation in modulating the DNA repair function of PNKP was previously investigated (21,31). To identify additional post-translational modification in PNKP, FLAG-tagged PNKP from stably expressing HEK293 cells (either mock-treated or treated with the radiomimetic drug, Bleomycin, to induce DSBs) was affinity purified and analyzed by mass spectrometry. PNKP was found to undergo post-translational acetylation at two different lysine residues (K142 and K226), as detected in peptide fragments, R/**K142/226**SNPGWENLEK and R/G**K142/226**LPAEEFK/A, by tandem mass spectrometry (**Fig. 1A**; **Supplementary Fig. 1A and B**). K142 acetylation (AcK142) was constitutive and detected in both control and Bleo-treated cells, whereas K226 acetylation (AcK226) was induced only upon Bleo treatment. PNKP domains are well characterized (6,32-34), and these two acetylation sites were found to be in distinct domains: AcK142 in the linker region (111-144 aa), whereas AcK226 in the phosphatase domain (145-336 aa) (**Fig. 1B)**. Additionally, to authenticate AcK142 and AcK226 sites in PNKP and the differential mode of their acetylation, the MS analysis of affinity-purified PNKP from WT and K226R (acetylation-deficient mutant) PNKP expressing HEK293 cell lines was

performed following mock and Bleo-treatment. The results confirmed PNKP acetylation in both control and Bleo-treated WT and K226R cell lines at the K142 site. However, AcK226 was observed in the WT cell line only following Bleo-treatment and no such acetylation was observed in the K226R mutant cell line (**Supplementary Fig. 1C)**. These data further confirmed two acetylation sites in PNKP of which K142 is acetylated constitutively in cell lines irrespective of any DNA damage-inducing treatment, whereas, K226 acetylation is induced by the DNA DSB-inducing agent, Bleomycin.

Site-specific acetylated lysine antibodies validate the acetylation of PNKP at K142 and K226

To validate MS-identified PNKP acetylation, we custom-generated PNKP acetylation site-specific Abs against individual peptide fragments containing acetylated K142 or K226 and validated such antibodies for target specificity by immunopulldown (IP) of acetylated PNKP from chromatin fraction of FLAG-tagged WT and acetylation-deficient (K142R or K226R) PNKP expressing HEK293 cells. Acetylated PNKP was identified by Western blot using anti-FLAG ab. Next, we performed indirect immunofluorescence using Ac-specific Abs to detect individual acetylation events in these cell lines. For this purpose, cells were either treated with Glucose oxidase (GO) to induce SSBs or Bleomycin to induce DSBs. We confirmed the presence of DSB markers, phospho-p53-binding protein 1 (p-53BP1) **(Supplementary Fig. 2A, lanes 1-2, top panel)** and γH2AX **(Supplementary Fig. 2A, lanes 1-2, 3rd panel from the top)** in Bleo-treated WT and K226R cells but not in GO-treated WT and K142R **(Supplementary Fig. 2A, lanes 3-4)** cells. All the microscopic experiments were performed following depletion of endogenous PNKP by 3'-UTR specific siRNA to exclude the possibility of any interference of acetylation from endogenous PNKP **(Supplementary Fig. 2B)**. The immunopulldown of PNKP with anti-AcK142 Ab followed by immunoblot using anti-FLAG ab showed the AcK142 PNKP only in WT but not in K142R cells (post GO treatment) **(Fig. 2A).** Indirect immunofluorescence analysis of the individual cell population using anti-AcK142 Ab demonstrated the nuclear localization of AcK142 PNKP in WT **(Fig. 2B, top panel)** and K226R **(Fig. 2B, bottom panel)** cell lines, but not in the K142R **(Fig. 2B, middle panel)** cell line. Therefore, both the IP-immunoblot and microscopic imaging data demonstrated the K142-specific constitutive acetylation in PNKP in the resting cells. Similarly, immunoprecipitation of PNKP with anti-AcK226 Ab showed that K226 acetylated PNKP exists only in the Bleo-treated WT cells **(Fig.**

2C, lane 3, upper panel). Neither the mock **(**both WT, **Fig. 2C, lane 1** and K226R, **lane 2)** nor the Bleo-treated K226R **(Fig. 2C, lane 4)** cells show the presence of AcK226. In microscopic imaging, we observed K226-specific acetylated PNKP only in Bleo-treated WT **(Fig. 2D, 2nd panel from the top)** cells, but not in WT mock **(Fig. 2D, top panel)** or mock **(Fig. 2D, 3rd panel from the top)** and Bleo-treated K226R **(Fig. 2D, bottom panel)** cell lines. These experimental findings confirmed DSB-induced acetylation of PNKP at K226 residue. To further confirm this, we performed a DSB-repair time course experiment following Bleo treatment in WT-PNKP expressing stable HEK293 cells. Our previous reports showed complete repair of DSBs in 12-16 h following Bleo-mediated DSB induction (17-19). Thus, we followed the K226 acetylation kinetics by immunofluorescence at 3, 6, and 9 h post-Bleo treatment using anti-AcK226 Ab. We indeed found that the acetylation at K226 was significantly reduced at 9 h **(Fig. 2E, bottom panel)**, indicating a reversal of K226 acetylation with the progression of DSB repair. This not only confirmed DSB-induced acetylation but also highlighted the reversible nature of the K226 acetylation event in PNKP.

p300 acetylates PNKP at lysine 142 and CBP at lysine 226

CBP and p300 are two major histone acetyltransferases (HATs) responsible for the acetylation of the vast majority of proteins *in vivo* (35-37). To explore any potential role of these HATs in the acetylation of PNKP in mammalian cells, we individually depleted the endogenous p300 **(Supplementary Fig. 3A)** and CBP **(Supplementary Fig. 3B)** in HEK293 cells using commercially available siRNAs, followed by indirect immunofluorescence using acetylation-specific Abs to assess the acetylation status at distinct residues. Immunofluorescence with anti-Ac-K142 Ab revealed the presence of AcK142 PNKP in control siRNA-transfected mock / GO-treated **(Fig. 3A, Top two panels, respectively)** HEK293 cells. AcK142 PNKP was also observed in the nucleus of CBP-depleted HEK293 cells but not in p300-depleted cells **(Fig. 3A, Bottom two panels, respectively).** This clearly indicated that the acetylation of PNKP at lysine 142 residue is mediated by p300, but not by CBP. Similarly, immunofluorescence with anti-Ac-K226 Ab showed the presence of AcK226 PNKP in control siRNA/Bleo-treated **(Fig. 3B, 2nd panel from the top)** cells but not in control siRNA/mock-treated cells **(Fig. 3B, top panel)**, consistent with our earlier observation of DSB-induced K226 acetylation. Most importantly, no such acetylation of PNKP was observed in CBP depleted/ Bleo-treated cells **(Fig. 3B 3rd panel from the top)**, unlike in p300 depleted/Bleo-treated cells **(Fig. 3B, bottom panel)**. This finding

confirmed that the DSB-induced acetylation of PNKP at K226 is mediated by CBP but not by p300. Overall, these experiments unveil the role of p300 and CBP in two distinct site-specific acetylation events of PNKP, viz., K142 and K226, respectively.

Acetylation of PNKP at K226 caused modest activation of its 3'-phosphatase but not kinase activity

PNKP can convert 5'-hydroxyl and 3'-phosphate termini to a canonical 5'-phosphate and 3'-hydroxyl moiety, respectively, which enables the gap-filling and ligation of damaged DNA (6-10). Thus, we explored the effect of these acetylation events on PNKP's 3'-phosphatase and 5'-kinase activities using affinity-purified FLAG-PNKP from control vs. Bleo-treated stable cell lines (WT, K142R, K226R and K142R/K226R). Bleo-induced DSB generation was confirmed by the expression of DSB marker, γH2AX in chromatin fraction of WT **(lanes 1-2)** and mutant **(lanes 3-4,** K142R**; lanes 5-6,** K226R; and **lanes 7-8,** K142R/K226R**)** FLAG-PNKP expressing cells **(Fig. 4A, upper panel)**. PNKP was IP'd from the same extract with anti-PNKP (total) Ab and immunoblotted with anti-FLAG Ab to confirm the similar level of FLAG-PNKP expression in these cell lines following mock/Bleo-treatment **(Fig. 4B)**. Assessment of 3'-phosphatase activity **(schematically shown in Fig. 4C)** revealed a moderate activation of PNKP in WT **(lanes 3 vs. 2)** and K142R **(lanes 5 vs. 4)** cells (K226 acetylation proficient) following Bleo-treatment, whereas no significant change of activity was observed in Bleo-treated K226R **(lanes 7 vs. 6)** and K142R/K226R **(lanes 9 vs. 8)** PNKP expressing cells **(Fig. 4D)**, where K226 acetylation was impaired. Thus, it is implied that modest activation of PNKP's 3'-phosphatase activity is mediated by K226 acetylation whereas constitutive K142 acetylation did not affect PNKP's 3'-phosphatase activity. This is further confirmed by assessing the 3'-phosphatase activity of affinity-purified PNKP from WT vs. acetylation-mimic (K142Q, K226Q, K142/226Q) PNKP expressing resting cells that showed no difference in activity between them **(Fig. 4E)**. Additionally, we assessed 5'-kinase activity using affinity-purified PNKP from WT vs. acetylation-deficient (K-R) mutant cells and observed no difference in such activity among the cell lines $\pm$ Bleo **(Fig. 4F).** Overall, experimental findings clearly indicated that acetylation at K226 induces a mild activation of PNKP's phosphatase activity but not its kinase activity.

Acetylation at K142 plays a critical role in repairing SSBs in the transcribed genes

To investigate the role of K142 and K226 acetylated PNKP in SSB repair, WT, K-R (acetylation-deficient) and K-Q (acetylation-proficient/mimic) mutant PNKP expressing cells were treated with Glucose Oxidase (GO) to induce SSBs, and the strand-break accumulation was analyzed in transcribed (HPRT, PolBeta and RNA polII) vs. non-transcribed (NANOG, OCT4 and MyH2) genes using long-amplicon qPCR (LA-qPCR) (17,18) after the cells were allowed to recover for 4 h following DNA damage induction. Also, to specifically assess the role of ectopically expressing PNKP in DNA SSB repair, prior depletion of endogenous PNKP was performed in these cells by 3' UTR specific siRNA **(Supplementary Fig. 4A; supplementary Fig. 4B)**. It was found that SSB repair of transcribed genes occurred in WT **(lanes 1-3, upper panel, Fig. 5A)** and K226R **(lanes 7-9, upper panel, Fig. 5A)** cells, but repair was abrogated in K142R **(lanes 4-6, upper panel, Fig. 5A)** and K142/226R **(lanes 10-12, upper panel, Fig. 5A)** mutant PNKP expressing cells. Interestingly, SSB repair was not affected in non-transcribed gens **(lower panel, Fig. 5A)** and we observed almost complete repair in WT (lanes 1-3), K142R (lanes 4-6), K226R (lanes 7-9) and K142/226R (lanes 10-12) cell lines. These findings are consistent with our earlier reports of PNKP's involvement in the preferential repair of transcribed genes (17-19). Thus, we conclude that in transcribed genes, the repair of GO-induced SSBs indeed relies only on K142 acetylation but not on K226 acetylation. This was corroborated with our further observation of complete repair of transcribed genes in all acetylation-mimic (K-Q) PNKP-expressing cells compared to WT **(Fig. 5B)**. Based on these data, it was imperative that AcK142 PNKP plays a critical role in the transcription-coupled SSB repair pathway.

Preferential repair of DSBs in the transcribed genes requires acetylation at K226 of PNKP

To further understand the functional significance of the two distinct acetylated residues (K142 and K226) of PNKP in SSB vs. DSB repair, we assessed the DNA strand-break accumulation in WT and mutant (K-R and K-Q PNKP expressing cells by LA-qPCR after the cells were treated with Bleo (to induce DSBs predominantly) and allowed 12-16 h for repair. Also, the effect of endogenous PNKP on the DNA repair was overcome by 3'-UTR specific siRNA mediated depletion of the same **(Supplementary Fig. 5A, B)**. We observed significant DNA strand break accumulation in both transcribed **(upper panel, Fig. 6A)** and non-transcribed **(lower panel, Fig. 6A)** genes in all these cell lines after Bleo treatment. However, DNA SBs were almost completely repaired in WT **(lanes 1-3)** cells, whereas K142R **(lanes 4-6)**, K226R **(lanes 7-9)** and K142/K226R **(lanes 10-12)** mutant PNKP expressing cells showed persistence of DNA SBs in

the transcribed genes **(upper panel, Fig. 6A)**. In contrast, almost complete repair of DNA strand breaks was observed in non-transcribed genes in K142R **(lanes 4-6)**, K226R **(lanes 7-9)** and K142/K226R **(lanes 10-12)** mutant cells **(Fig. 6A, lower panel)**. Thus, it is implied that acetylated (both K142 and K226 specific) PNKP preferentially repaired the transcribed genes. Since there will be a mixed population of SSBs and DSBs following Bleo treatment (38-40), hence, K142R mutant expressing cells also showed persistence of DNA SBs due to impairment of K142 acetylation mediated SSB repair. Since K226R PNKP expressing cells accumulate DNA SBs, unlike as we observed following GO-mediated SSB induction and subsequent repair, it is evident that acetylation at the K226 site is involved primarily in DSB repair. Interestingly, in K-Q mutant (acetylation mimic) expressing cells, complete repair of the DNA strand break was observed **(Fig. 6B)**. Thus, based on overall experimental findings, we conclude that AcK142 PNKP is primarily involved in SSB repair and K226 acetylated PNKP plays a major role in the DSB repair pathway. Our lab previously showed the formation of R-loop (RNA-DNA hybrid) at DSB sites following Bleo-treatment (17-19). We further reported the association of PNKP with such R-loops to facilitate RNA-templated DSB repair and resolution of the R-loops with repair progression. Thus, in an attempt to investigate the cause of abrogated repair of Bleo-induced SBs in acetylation-deficient cells, we assessed the level of such R-loop formation and their resolution in the mutant K226R PNKP-expressing cells compared to their WT counterpart. Genomic DNA isolated from WT and K226R cells (both mock and Bleo-treated) at 16 h post-treatment, was subjected to Slot-blot analysis using S9.6 RNA-DNA hybrid-specific Ab. Results showed increased R-loop formation in Bleo-treated WT and K226R cells indicating RNA-DNA hybrid formation. These R-loops were significantly resolved in WT but persisted in K226R mutant PNKP-expressing cells (**Fig. 6C**), indicating a probable impairment of RNA-templated DSB repair in the acetylation-deficient PNKP-expressing cells. Thus, we speculate that acetylated PNKP is involved in RNA-templated error-free repair and the unresolved R-loop is most likely one of the principal causes of abrogated DNA repair in Bleo-treated K226R mutant cells. The persistence of R-loops has been suggested to induce DNA damage and genomic instability resulting in considerable cell toxicity (41-44). Thus, in view of persistent R-loop formation and abrogated DNA strand-break repair in mutant PNKP-expressing cells, we investigated the LDH cytotoxicity assay following Bleo-treatment. Results indeed showed a substantial increase of

LDH release in mutant cells compared to WT **(Fig. 6D),** indicating significant cell toxicity under acetylation-deficiency conditions.

Preferential association of acetylated PNKP with the transcribed regions

Based on our experimental findings so far, we hypothesize that K142 acetylation of PNKP plays a role in SSB repair whereas K226 acetylation is involved in DSB repair. In our earlier studies, we provided evidence of pre-formed, pathway-specific DNA repair complexes in mammalian cells (17-19). Thus, we addressed the question of whether AcK142 PNKP and AcK226 PNKP might interact and make a complex exclusively with SSBR and DSBR protein(s), respectively for their recruitment to the transcribed region. To investigate this, we performed Co-IP from the chromatin fraction using anti-AcK142 or anti-AcK226 Abs to characterize the immunocomplex of acetylated PNKP in WT-PNKP expressing stable cell lines (± GO or Bleo, respectively). Results indeed showed the presence of RNAP II, along with SSB repair proteins DNA Lig III and XRCC1 in the AcK142 PNKP immunocomplex, whereas DSB repair proteins, XRCC4 and DNA Lig IV were absent in this immunocomplex **(Fig. 7A)**. On the contrary, we observed RNAP II, DNA Lig IV, Ku70 and XRCC4, but not the SSB repair proteins (DNA Lig III and XRCC1) in the AcK226 PNKP immunocomplex following Bleo-treatment **(Fig. 7B)**. Importantly, we could specifically detect p300 and CBP in the K142 and K226 immunocomplexes, respectively, consistent with our microscopic imaging data. These data further demonstrated the respective roles of PNKP acetylation at K142 and K226 residues on SSB and DSB repair pathways. Since the Ac-PNKP preferentially repaired the transcribed genes, we examined the genomic association of AcK142 or AcK226 PNKP by performing chromatin immunoprecipitation (ChIP) on soluble chromatin preparations of WT-PNKP expressing stable cells (± GO or Bleo, respectively) using the AcK142 or AcK226 PNKP Abs. We observed the preferential recruitment of both AcK142 and AcK226 PNKP in the coding region of transcribed genes (HPRT, ACTB and POLR2A) but not in the non-transcribed genes (NANOG, OCT4 and MyH2) (Fig. 7C-D). From these findings, we conclude that in the event of SSB and DSB, AcK142 and AcK226 PNKP individually interact and make complexes with SSB and DSB repair proteins, respectively, and are preferentially recruited to the coding region of the transcribed genes to facilitate repair.

PNKP acetylation at K226 is impaired in Huntington's Disease (HD) mouse-derived striatal neuronal cells (Q111)

Several earlier studies, including ours, have shown the specific degradation of CBP in HD (both cell culture and mouse models) (24,45-47). In this study, microscopic imaging data on CBP-mediated acetylation of PNKP at K226 in the cell culture model inspired us to explore the PNKP acetylation pattern at K142 and K226 in Huntington's disease (HD) to gain more insight into the significance of such acetylation events in HD pathology. For this purpose, we used the WT and HD mouse-derived striatal neuronal cells with normal and expanded polyQ repeats (Q7 and Q111, respectively) (48). Since Q111 cells are derived from the HD mouse model, which shows all signs and symptoms of aggressive HD, assessment of the acetylation status of PNKP in this cell line compared to Q7 cells can be reliably correlated with the diseased vs. healthy conditions. Indirect immunofluorescence analysis using anti-AcK142 Ab in mock/GO-treated Q7 and Q111 cells showed the presence of acetylated PNKP in both Q7 **(Fig. 8A, top panel and 2nd panel from the top)** and Q111 **(Fig. 8B, top panel and 2nd panel from the top)** cells. On the contrary, similar microscopic imaging using anti-AcK226 Ab in mock/Bleo-treated cells showed the presence of acetylated PNKP only in Bleo-treated Q7 **(Fig. 8A, bottom panel)** cells. We could not detect any AcK226 PNKP in mock-treated Q7 cells as expected **(Fig. 8A, 3rd panel from the top)**. More interestingly, Bleo-treated Q111 **(Fig. 8B, bottom panel)** cells did not show acetylation of K226 residue, unlike Q7 cells, indicating impairment of such acetylation event in Q111 cells. We further assessed the level of CBP,p300, γH2Ax and PNKP in the chromatin fraction of Q7 and Q111 cells by immunoblotting using specific Abs. We observed a comparable level of p300 and PNKP **(Fig. 8C, second and third panels from top)** in both Q7 and Q111 but a significantly reduced level of CBP **(Fig. 8C, top panel)** in Q111 compared to Q7 cells. This data is consistent with our previous finding in the HD mouse and patient-derived iPSC cells (24). It further corroborated with the microscopic imaging data showing the presence of AcK142 PNKP in both Q7 and Q111 cells (as the p300 level is comparable) and impairment of Bleo-induced acetylation of K226 residue of PNKP in Q111 cells due to CBP degradation. Finally, we studied the DNA damage accumulation in Q7 vs. Q111 cells in three representative transcribed genes (POLB, TUBB and NeuroD) and three non-transcribed genes (MyH4, MyH6 and MyoD) by LA-qPCR. Results showed a progressive and significant DNA strand break accumulation in transcribed genes (POLB, TUBB and NeuroD) in Q111 cells compared to Q7 cells **(Fig. 8D, E)**. Consistently a significantly increased level of γH2Ax in Q111 compared to Q7 (**Fig. 8C, fourth panel from top)** confirmed the DSB accumulation in Q111 cells. This data is also consistent

with our earlier report of the accumulation of DNA SBs in transcribed genes in HD and further provided a mechanistic basis for DNA damage accumulation in HD due to a lack of CBP-mediated K226 acetylation of PNKP.

Discussion

The acetylation of protein is one of the most dominant post-translational modifications in eukaryotes and has a profound effect on the functional properties of multiple proteins that ultimately impact cellular physiology (49,50). Several human DNA replication and repair enzymes, involved in major DNA repair pathways, including mismatch repair (MMR), BER, nucleotide excision repair (NER), homologous recombination (HR), and NHEJ have been shown to be acetylated (5,11,13,28,51,52). Moreover, reversible acetylation of these proteins has been shown to play a key role in DNA binding affinity, transcriptional activation, protein stability and protein-protein interactions (53-55). Mitra's group has previously reported the acetylation of several DNA repair enzymes involved in the BER pathway, such as NEIL1, NEIL2, OGG1 and APE1 (53-56). All these acetylation events have diverse effects on the repair activity of the acetylated proteins. For instance, oxidative stress-induced acetylation significantly increases OGG1's activity in the presence of AP-endonuclease by reducing its affinity for the product abasic (AP) site (56). Acetylation of NEIL2 inactivates its glycosylase/AP lyase activity (54), whereas acetylation of NEIL1 stabilizes the formation of chromatin-bound repair complexes that protect cells from oxidative stress (53). Acetylated NEIL1 preferentially associates with euchromatin and maintains transcribed genome integrity (57). NEIL2 is also involved in TC-BER; however, whether acetylation or any other modification plays any role in the involvement of NEIL2 in such repair pathway warrants further investigation.

NEIL-initiated TC-BER pathway requires PNKP to process the 3'-P termini, one of the most abundant blocked termini at the site of DNA strand breaks. It has been shown that ionizing radiation (IR)-induced phosphorylation of PNKP, mediated by DNA-PKcs and ATM at selective serine residues, enhances its association with XRCC4-Lig IV and increases its DNA binding and phosphatase/kinase activities (21). Such modifications are important for the dynamic assembly of PNKP with other DNA repair proteins in the complex but may not be the determining factor for the pathway choice of PNKP. We postulated that other types of post-translational modifications (PTM(s)) could effectively modulate PNKP's role in TC-BER/SSBR vs. TC-NHEJ. Here we report identification of two acetylation sites (K142 and K226) in PNKP and demonstrated that

acetylation at K142 occurs constitutively and at K226, only after Bleo-induced DSB formation. Despite the acetylation deficient (K142R and K226R) as well as acetylation mimic (K142Q and K226Q) mutants having comparable enzymatic activity with that of WT PNKP, K142R and K226R expressing cells showed DNA damage accumulation in the transcribed genes only. However, acetylation mimics K142Q and K226Q mutants can efficiently repair transcribed genes. Moreover, our ChIP data suggest a preferential association of the acetylated PNKP with the transcribed genome, clearly indicating that acetylation of PNKP plays an important role in transcribed genome repair. These results are consistent with our earlier reports demonstrating PNKP's preferential role in the repair of SSBs and DSBs in the transcribed genes (14,15,17,18).

Two major acetyltransferases, p300 and the transcriptional co-activator, CREB binding protein (CBP) are highly homologous (58-60) and both proteins are indispensable for development (61). While there is evidence of tissue-specific non-redundancy, in most cases CBP and p300 are considered to be functionally identical. We and others previously reported that p300 acetylates most of the DNA repair proteins involved in the BER process, such as FEN 1, Polβ, TDG, NEIL1, NEIL2, APE1 and PCNA and modulate their activity suggesting that acetylation of repair proteins contributes to the regulation of the BER process (53-55,57,62,63). Some reports indicate that CBP also serves as an acetyl transferase for several DNA repair proteins, such as Ku70, PCNA, TDG as well as tumor suppressor, p53 (63). In this study, we show that PNKP, involved in multiple DNA repair pathways, is acetylated by both acetyl transferases, p300 and CBP, at two distinct lysine residues. It was found that p300 acetylates K142 constitutively and CBP acetylates at K226 only after DSB induction. We have previously shown that NEIL1 and NEIL2 stably associate with p300, forming specific BER complexes along with PNKP (53,54,57). Association of AcK142 with TC-BER/SSBR proteins, elongating form of RNA polymerase II and specifically with p300 is therefore consistent with our previous reports. Interestingly, in the Ac-K142 PNKP immunocomplex, we could detect the presence of a NHEJ protein, Ku70. This is corroborative with a recent report that shows BER-NHEJ cross-talk mediated by the formation of a Ku70-Polβ complex at the repair foci and impairment of BER efficiency by ablation of Ku70 (68). Notably, we found association of K226 with CBP, RNAP II and NHEJ factors following DSB induction. To our knowledge, this is the first example of acetylation of a DNA repair protein at two distinct sites by two different acetyl transferases, where such modifications act as a critical determinant of PNKP's role in SSBR vs.

NHEJ. Additionally, DSB-induced Ac-K226 PNKP immunocomplex showed the presence of a RT-polymerase, DNA Pol η. We have recently provided evidence in favor of the critical role of Pol η in copying the sequence information from nascent RNA into DNA at the DSB sites (19). Since acetylation-deficient K226R cells show accumulation of R-loops at the DSB sites, we postulate a role of Ac-K226 PNKP in the recruitment of Pol η for RNA-templated error-free repair of DSBs via the TC-NHEJ pathway.

Mutations in PNKP and resulting repair deficiency have been implicated in a variety of human neurological diseases, such as MCSZ, AOA4, etc (28,64-67). We have recently shown that a point mutation of PNKP leads to abrogation of its nuclear localization resulting in AOA4 in humans (22). We also showed that PNKP activity, not its expression level, is severely abrogated in SCA3 and HD, the two major poly glutamine diseases (18,24). Several reports, including ours, have shown selective degradation of CBP, but not p300, in HD (45-47). We indeed found that K142, but not K226, is acetylated in mouse Huntington's Disease (HD) derived striatal neuronal cells (Q111), which is consistent with provious report and our present study showing selective degradation of CBP in HD mouse striatal neuronal cells (Q111) compared to WT cells (Q7). Moreover, Q111 cells showed progressive accumulation of DSBs in the transcribed genes, which can trigger apoptosis to vulnerable brain cells: a plausible cause of the neurodegenerative feature in HD. Interestingly, our results suggest accumulation of DNA SBs, preferentially in the transcribed genes, in cells where the K226 acetylation site is mutated by a non-acetylable residue. Thus, the preferential accumulation of DNA SBs in transcribed genes of K226R mutant expressing cells as well as in K226 acetylation-deficient HD cells is internally consistent. In summary, we have provided critical evidence for the role of acetylation at two distinct residues located in different domains of PNKP that regulate its functionally distinct roles in TC-BER/SSBR vs. TC-NHEJ in mammalian cells.

Acknowledgments

This work was supported by National Institute of Health Grants 2R01 NS073976 to TH, R01HL145477 to TH and Sanjiv Sur (SS), Division of Allergy and Clinical Immunology, Baylor College of Medicine, Houston, National Institute of Allergic and Infectious Diseases (NIAID) grant AI062885 to IB and University of California Tobacco-Related Disease Research Program

(TRDRP) grant 26IR-0017 to A.H.S. We thank Dr. Katherine Kaus, Research Development Specialist at the University of Texas Medical Branch for editing this manuscript.

Author contributions

TH conceived the research. TH, AI and AC designed the research. AI, AC, AS and UA performed research. IB and GS provided reagents and critical intellectual inputs. AI, AC and TH wrote the manuscript. All the authors read and approved the final version of the manuscript.

Conflict of interest

The authors declare that they do not have any conflicts of interest.

Data availability

The data that support the findings of this study are available from the corresponding author upon request.

Figure legends

Main Figures

Figure 1. Acetyl-lysine-containing peptides in PNKP identified by LC-MS/MS. (A) Acetylation sites are marked in red within the peptide sequence and the amino acid residues are marked in a subtitle as well. The table shows the sequest algorithm scores (Xcorr and ΔCorr) along with the mass accuracy measurement of the acetylated peptides. (B) Schematic representation of PNKP domains (FHA, Linker, phosphatase and kinase domains), indicating the K142 acetylation site in the linker region and the K226 acetylation site in the phosphatase domain.

Figure 2. Detection of AcK142 and AcK226 PNKP in the chromatin fraction of stable cell lines by anti-AcK (K142 or K226) specific Abs. (A) PNKP was IP'd using the anti-AcK142 Ab from the chromatin fraction of Glucose oxidase-treated WT (lane 1) and K142R mutant (lane 2) cells and was probed with anti-FLAG Ab (Upper Panel). Lower Panel: Input showing similar ectopic expression of PNKP-FLAG in the cell lines as detected with anti-FLAG Ab. (B) Indirect immunofluorescence to detect nuclear localization of AcK142 PNKP in WT vs. mutant cell lines. Stable cell lines expressing WT and mutant PNKP proteins were transfected with 3'-UTR-specific siRNA to deplete endogenous PNKP. Glucose oxidase (GO) treated cells were fixed, permeabilized, and stained with an anti-Ac-K142 Ab. Nuclei were counterstained with DAPI.

Microscopic images were acquired individually using blue (461 nm) and red (594 nm) fluorescent conditions and images of two colors were merged, and pictures were taken at 40 µm area as shown in the figure. (C) PNKP was IP'd using the anti-AcK226 Ab from the chromatin fraction of mock (lanes 1, 2) and Bleomycin (Bleo)-treated (lanes 3, 4) WT (lanes 1, 3) and K226R mutant (lanes 2, 4) cells and was probed with anti-FLAG Ab (Upper Panel). Lower Panel: Inputs showing similar ectopic expression of PNKP-FLAG in the cell lines detected with anti-FLAG Ab. (D) Stable cell lines expressing WT and mutant K226R PNKP proteins were transfected with 3'-UTR-specific siRNA to deplete endogenous PNKP. Mock- or Bleomycin-treated cells were fixed, permeabilized, and stained with an anti-Ac-K226 Ab. Nuclei were counterstained with DAPI. Nuclear localization of K226 acetylated PNKP in WT and mutant cell lines were shown individually in the figure. (E) Indirect immunofluorescence to check the status of K226 acetylated PNKP in mock vs. Bleo-treated WT-PNKP expressing cells at 3 h, 6 h and 9 h post-Bleo treatment. All other conditions were the same as described above.

Figure 3. (A) The status of K142 specific PNKP acetylation in control siRNA vs. CBP/p300 siRNA transfected and mock/GO-treated HEK293 cells by indirect immunofluorescence using anti-acetyl lysine (K142) PNKP Ab. Nuclear DAPI staining, Texas red Ab staining, and the overlay were shown side by side in three separate panels. (B) The status of K226-specific PNKP acetylation in control siRNA vs. CBP/p300 siRNA transfected, and + Bleo-treated HEK293 cells was determined by fluorescence microscopic imaging using anti-acetyl lysine (K226) PNKP Ab. All other conditions were the same as described in (A).

Figure 4. Assessment of the effect of acetylation on PNKP's 3'-phosphatase and 5'-kinase activities (A). Western blot shows expression of DSB marker, γH2Ax (upper panel) in the chromatin fraction of WT (lanes 1, 2), K142R (lanes 3, 4), K226R (lanes 5, 6) and K142/226R (lanes 7, 8) post mock (-) or Bleo (+) treatment. HDAC2 is used as the chromatin fraction loading control (lower panel). (B) Twenty µL IP'd and FLAG-peptide eluted PNKP was loaded in gradient gel and immunoblotted with anti-FLAG Ab to determine the level of IP'd WT and mutant PNKP (upper panel) and 10 µg of chromatin fraction of WT and mutant PNKP was used as an input (lower panel). (C) A schematic representation of PNKP's 3'-phosphatase assay. (D) 3′-phosphatase assay of IP'd PNKP from WT (lane 2-3), K142R (lane 4-5), K226R (lane 6-7) and K142/226R (lane 8-9) cells post mock (-) or Bleo (+) treatment. Lane 1: No protein (NP),

substrate only. Lower Panels: Quantitation of the products (% of released phosphate) is represented in the bar diagram (n=3, *P<0.05 between mock (-) and Bleo (+) treatment in WT and K142R; ns: non-significant, P>0.05). (E) Similar phosphatase assay of IP'd PNKP from WT (lane 1), K142Q (lane 2), K226Q (lane 3) and K142/226Q (lane 4). NP: no protein, substrate only. Lower Panels: Quantitation of the products (% of released phosphate) is represented in the bar diagram (n=3, ns: non-significant, P>0.05). (F) 5′-kinase assay of IP'd PNKP from WT (lane 1-2), K142R (lane 3-4), K226R (lane 5-6) and K142/226R (lane 7-8) post mock (-) or Bleo (+) treatment. M: radiolabeled 32 nt marker. NP: No protein, substrate only. Quantitation of the products (% phosphorylated product) is represented in the bar diagram (n=3, ns=non-significant, P>0.05). In each case of (D-F), S: Substrate and P: product.

Figure 5. Role of lysine 142 specific acetylated PNKP on SSB repair determined by LA qPCR. (A) (Upper panels) Representative gel images of long amplicon qPCR assay showing each long amplicon (10–12 kb) and a short amplicon (~200–300 bp) of the transcribed (HPRT, PolBeta, and RNA polII) genes and non-transcribed (NANOG, OCT3/4 and MyH2) from the DNA isolated from WT (lanes 1-3), K142R (lanes 4-6), K226R (lanes 7-9) and K142/226R (lanes 10-12) cells either mock (C) or GO- treated (G) or at 4 h recovery (R) following GO treatment. (Lower Panels) The bar diagrams represent the normalized (with short PCR amplicon) relative band intensity with the mock-treated control (C) arbitrarily set as 100 (n=3, ***P<0.005) for each cell line. (B) Similar LA-qPCR assay of the transcribed (HPRT, PolBeta, and RNA polII) genes was performed in WT (lanes 1-3), K142Q (lanes 4-6), K226Q (lanes 7-9) and K142/226Q (lanes 10-12) cells under similar treatment conditions as described above. All LA-qPCR experiments were performed following the depletion of endogenous PNKP in WT and mutant cells by 3'-UTR-specific siRNA.

Figure 6. Assessment of the effect of lysine 226 specific PNKP acetylation on repair of Bleo-induced DSBs by long amplicon qPCR. (Upper panels) Representative agarose gel images of the long amplicon (10–12 kb) and a short amplicon ((~200–300 bp) of the corresponding genes from WT (lanes 1-3), K142R (lanes 4-6), K226R (lanes 7-9) and K142/226R (lanes 10-12) cells either mock (C) or Bleo-treated (B) or at 16 h recovery (R) following Bleo-treatment. (Lower Panels)

The bar diagrams represent the normalized (with short PCR amplicon) relative band intensity with the mock-treated control (C) arbitrarily set as 100 (n=3, ***P<0.005; ns: non-significant, P>0.05) for each cell line. (B) Similar LA-qPCR assay of the transcribed (HPRT, PolBeta, and RNA polII) genes was performed in WT (lanes 1-3), K142Q (lanes 4-6), K226Q (lanes 7-9) and K142/226Q cells under similar treatment conditions as described above. (C) Bar diagram shows quantification of R-loop-specific signal normalized to dsDNA-specific signals in WT and K226R PNKP expressing stable cells following mock (C) or Bleo (B) treatment or at 16h post Bleo-treatment (R). Error bars show ±SD of the mean (n = 3, ***P < 0.005; ns: non-significant, P>0.05). (D) LDH release assay following Bleo-treatment in K142R, K226R and K142/226R mutant cells compared to WT. Bar graph represented the percent LDH release in WT and K-R mutant cells due to changes in membrane permeability by Bleo treatment. Error bars show ±SD of the mean (n = 3, ***P < 0.005). All LA-qPCR/R-loop/LDH assays were performed following the depletion of endogenous PNKP in WT and mutant cells by 3'-UTR-specific siRNA.

Figure 7. Assessment of K142 and K226 acetylated PNKP immunocomplexes and their recruitment to the transcribed region. Benzonase-treated chromatin fraction from the WT-PNKP-FLAG cells following mock (-)/GO (+) or mock (-)/Bleo (+) treatment was immunoprecipitated (IP'd) individually with (A) anti-Ac-K142 Ab or (B) Ac-K226 Ab, respectively along with control IgG (rabbit) Ab and probed with respective Abs as indicated to the right of the panels. The binding to the exonic regions of transcribed (POLR2A, HPRT, Actin B) vs. the non-transcribed (MyH2, Oct3, NanoG) genes were quantified by quantitative PCR (qPCR) from immunoprecipitated DNA from PNKP-FLAG stable cells ± GO or Bleo treatment using Ac-K142 (C) or Ac-K226 (D) Abs, respectively. The data are represented as fold enrichment of % input over IgG with mock-treated samples considered as unity. Error bars represent ±SD of the mean (n = 3). ***P < 0.005, **P < 0.01 represent statistical significance between mock and GO/Bleo treatment for each gene (ns, nonsignificant, P > 0.05).

Figure 8. The status of K142 and K226 specific PNKP acetylation and DNA strand break repair in WT mouse striatal neuronal cells (Q7) vs. Huntington's Disease (HD)-derived striatal neuronal cell (Q111). (A) Microscopic imaging of K142 specific acetylated PNKP ± GO treatment as well as K226 specific acetylated PNKP ± Bleo treatment in Q7 cells. Nuclear DAPI staining, Texas red Ab staining, and the overlay were shown side by side in three separate

panels. (B) Similar microscopic imaging in Q111 cells ±GO/Bleo using anti-AcK142 and AcK226 Abs. (C) Western blots to assess the levels of proteins (as indicated on the right) in the chromatin fraction of Q7 vs. Q111 cells. HDAC2: loading control. (D) LA-qPCR for determining the DNA strand break accumulation in transcribed (POLB, TUBB and NEUROD) and non-transcribed (MYH4, MYH6 and MYOD) genes in Q111 cells compared to Q7 cells. (Upper panels): Representative agarose gel images of the Long (LA) vs. Short (SA) amplicons from DNA from Q7 and Q111 cells at passage 5 (P5) and 9 (P9). (Lower panels): Bar diagrams show the normalized (with short PCR amplicon) relative band intensity with the Q7 control arbitrarily set as 100 (n=3, ***P<0.005, ns: non-significant, P>0.05).

Supplementary Figures:

Supplementary Figure 1. Identification of two novel acetyl lysine sites in PNKP by LC-MS/MS. The figure shows the fragmentation pattern of two acetylated peptides matched to PNKP. Representative figures of acetyl-lysine spectrums of PNKP are shown: (A) the spectrum of peptide sequence for K142 acetylation (B) the spectrum of peptide sequence for K226 acetylation**.** The acetylated lysines are shown as K#. The # symbol represents a mass addition of 42.0106 Da to lysine. (C) Results of a similar Mass Spectrometric analysis are represented in the table showing the acetylated residues in WT vs. K226R PNKP stable cell lines ±Bleo.

Supplementary Figure 2. (A) Western blot shows the expression level of phosphorylated 53BP1, total 53BP1 and γH2AX 2 in (the whole cell/chromatin fraction??) of Bleo-treated WT (lane 1) and K226R (lane 2) and Go-treated WT (lane 3) and K142R (lane 4) cells. HDAC2: used as loading control. (B) Depletion of endogenous PNKP by 3'-UTR specific siRNA. The representative agarose gel shows the extent of depletion of endogenous PNKP in WT, K142R, K226R and K142/226R PNKP expressing stable cell lines by 3'UTR specific siRNA. GAPDH was used as housekeeping control (upper panels). The bar diagram represents the relative expression level of endogenous PNKP normalized with the expression of endogenous control GAPDH and presented graphically as normalized relative band intensity with the control siRNA transfected samples considered as 100 arbitrarily (n=3, ***P<0.005) (lower panel).

Supplementary Figure 3. Depletion of endogenous CBP and p300 by siRNA in HEK293 cell lines. WB analysis shows the relative expression level of (A) p300 and (B) CBP in (whole

cell/chromatin fraction??) following control siRNA (Con; lane 1) and specific siRNA (lane 2) transfection. HDAC2 is used as a loading control.

Supplementary Figure 4. Depletion of endogenous PNKP by 3'-UTR specific siRNA. The representative agarose gels (upper panels) show the extent of depletion of endogenous PNKP in WT, K142R, K226R and K142/226R PNKP expressing stable cell lines (A) and WT, K142Q, K226Q and K142/226Q PNKP expressing stable cell lines (B) by 3'UTR specific siRNA. The bar diagrams represents the relative expression level of endogenous PNKP normalized with the expression of endogenous control GAPDH and presented graphically as normalized relative band intensity with the control siRNA transfected samples considered as 100 arbitrarily (n=3, ***P<0.005) (lower panels).

Supplementary Figure 5. Depletion of endogenous PNKP by 3'-UTR specific siRNA. (Upper panels) The representative agarose gels show the extent of depletion of endogenous PNKP in (A) WT, K142R, K226R and K142/226R PNKP expressing stable cell lines and in (B) WT, K142Q, K226Q and K142/226Q PNKP expressing stable cell lines under the same experimental conditions. (Lower panels) The bar diagram represents the relative expression level of endogenous PNKP normalized with the expression of endogenous control GAPDH and presented graphically as normalized relative band intensity with the control siRNA transfected samples considered as 100 arbitrarily (n=3, ***P<0.005).

References

1. Curtin, N. J. (2012) DNA repair dysregulation from cancer driver to therapeutic target. *Nat Rev Cancer* **12**, 801-817
2. McKinnon, P. J. (2017) Genome integrity and disease prevention in the nervous system. *Genes Dev* **31**, 1180-1194
3. Neil, A. J., Belotserkovskii, B. P., and Hanawalt, P. C. (2012) Transcription blockage by bulky end termini at single-strand breaks in the DNA template: differential effects of 5' and 3' adducts. *Biochemistry* **51**, 8964-8970
4. Chatterjee, N., and Walker, G. C. (2017) Mechanisms of DNA damage, repair, and mutagenesis. *Environ Mol Mutagen* **58**, 235-263
5. Jilani, A., Ramotar, D., Slack, C., Ong, C., Yang, X. M., Scherer, S. W., and Lasko, D. D. (1999) Molecular cloning of the human gene, PNKP, encoding a polynucleotide kinase

3'-phosphatase and evidence for its role in repair of DNA strand breaks caused by oxidative damage. *J Biol Chem* **274**, 24176-24186

6. Karimi-Busheri, F., Daly, G., Robins, P., Canas, B., Pappin, D. J., Sgouros, J., Miller, G. G., Fakhrai, H., Davis, E. M., Le Beau, M. M., and Weinfeld, M. (1999) Molecular characterization of a human DNA kinase. *J Biol Chem* **274**, 24187-24194
7. Chatterjee, A., Saha, S., Chakraborty, A., Silva-Fernandes, A., Mandal, S. M., Neves-Carvalho, A., Liu, Y., Pandita, R. K., Hegde, M. L., Hegde, P. M., Boldogh, I., Ashizawa, T., Koeppen, A. H., Pandita, T. K., Maciel, P., Sarkar, P. S., and Hazra, T. K. (2015) The role of the mammalian DNA end-processing enzyme polynucleotide kinase 3'-phosphatase in spinocerebellar ataxia type 3 pathogenesis. *PLoS Genet* **11**, e1004749
8. Freschauf, G. K., Karimi-Busheri, F., Ulaczyk-Lesanko, A., Mereniuk, T. R., Ahrens, A., Koshy, J. M., Rasouli-Nia, A., Pasarj, P., Holmes, C. F., Rininsland, F., Hall, D. G., and Weinfeld, M. (2009) Identification of a small molecule inhibitor of the human DNA repair enzyme polynucleotide kinase/phosphatase. *Cancer Res* **69**, 7739-7746
9. Freschauf, G. K., Mani, R. S., Mereniuk, T. R., Fanta, M., Virgen, C. A., Dianov, G. L., Grassot, J. M., Hall, D. G., and Weinfeld, M. (2010) Mechanism of action of an imidopiperidine inhibitor of human polynucleotide kinase/phosphatase. *J Biol Chem* **285**, 2351-2360
10. Meijer, M., Karimi-Busheri, F., Huang, T. Y., Weinfeld, M., and Young, D. (2002) Pnk1, a DNA kinase/phosphatase required for normal response to DNA damage by gamma-radiation or camptothecin in Schizosaccharomyces pombe. *J Biol Chem* **277**, 4050-4055
11. Das, A., Wiederhold, L., Leppard, J. B., Kedar, P., Prasad, R., Wang, H., Boldogh, I., Karimi-Busheri, F., Weinfeld, M., Tomkinson, A. E., Wilson, S. H., Mitra, S., and Hazra, T. K. (2006) NEIL2-initiated, APE-independent repair of oxidized bases in DNA: Evidence for a repair complex in human cells. *DNA Repair (Amst)* **5**, 1439-1448
12. Hazra, T. K., and Mitra, S. (2006) Purification and characterization of NEIL1 and NEIL2, members of a distinct family of mammalian DNA glycosylases for repair of oxidized bases. *Methods Enzymol* **408**, 33-48
13. Wiederhold, L., Leppard, J. B., Kedar, P., Karimi-Busheri, F., Rasouli-Nia, A., Weinfeld, M., Tomkinson, A. E., Izumi, T., Prasad, R., Wilson, S. H., Mitra, S., and Hazra, T. K. (2004) AP endonuclease-independent DNA base excision repair in human cells. *Mol Cell* **15**, 209-220
14. Banerjee, D., Mandal, S. M., Das, A., Hegde, M. L., Das, S., Bhakat, K. K., Boldogh, I., Sarkar, P. S., Mitra, S., and Hazra, T. K. (2011) Preferential repair of oxidized base damage in the transcribed genes of mammalian cells. *J Biol Chem* **286**, 6006-6016
15. Chakraborty, A., Wakamiya, M., Venkova-Canova, T., Pandita, R. K., Aguilera-Aguirre, L., Sarker, A. H., Singh, D. K., Hosoki, K., Wood, T. G., Sharma, G., Cardenas, V., Sarkar, P. S., Sur, S., Pandita, T. K., Boldogh, I., and Hazra, T. K. (2015) Neil2-null Mice Accumulate Oxidized DNA Bases in the Transcriptionally Active Sequences of the Genome and Are Susceptible to Innate Inflammation. *J Biol Chem* **290**, 24636-24648
16. Mandal, S. M., Hegde, M. L., Chatterjee, A., Hegde, P. M., Szczesny, B., Banerjee, D., Boldogh, I., Gao, R., Falkenberg, M., Gustafsson, C. M., Sarkar, P. S., and Hazra, T. K. (2012) Role of human DNA glycosylase Nei-like 2 (NEIL2) and single strand break repair protein polynucleotide kinase 3'-phosphatase in maintenance of mitochondrial genome. *J Biol Chem* **287**, 2819-2829

17. Chakraborty, A., Tapryal, N., Venkova, T., Horikoshi, N., Pandita, R. K., Sarker, A. H., Sarkar, P. S., Pandita, T. K., and Hazra, T. K. (2016) Classical non-homologous end-joining pathway utilizes nascent RNA for error-free double-strand break repair of transcribed genes. *Nat Commun* **7**, 13049
18. Chakraborty, A., Tapryal, N., Venkova, T., Mitra, J., Vasquez, V., Sarker, A. H., Duarte-Silva, S., Huai, W., Ashizawa, T., Ghosh, G., Maciel, P., Sarkar, P. S., Hegde, M. L., Chen, X., and Hazra, T. K. (2020) Deficiency in classical nonhomologous end-joining-mediated repair of transcribed genes is linked to SCA3 pathogenesis. *Proc Natl Acad Sci U S A* **117**, 8154-8165
19. Chakraborty, A., Tapryal, N., Islam, A., Sarker, A. H., Manohar, K., Mitra, J., Hegde, M. L., and Hazra, T. (2023) Human DNA polymerase eta promotes RNA-templated error-free repair of DNA double-strand breaks. *J Biol Chem* **299**, 102991
20. Segal-Raz, H., Mass, G., Baranes-Bachar, K., Lerenthal, Y., Wang, S. Y., Chung, Y. M., Ziv-Lehrman, S., Strom, C. E., Helleday, T., Hu, M. C., Chen, D. J., and Shiloh, Y. (2011) ATM-mediated phosphorylation of polynucleotide kinase/phosphatase is required for effective DNA double-strand break repair. *EMBO Rep* **12**, 713-719
21. Zolner, A. E., Abdou, I., Ye, R., Mani, R. S., Fanta, M., Yu, Y., Douglas, P., Tahbaz, N., Fang, S., Dobbs, T., Wang, C., Morrice, N., Hendzel, M. J., Weinfeld, M., and Lees-Miller, S. P. (2011) Phosphorylation of polynucleotide kinase/ phosphatase by DNA-dependent protein kinase and ataxia-telangiectasia mutated regulates its association with sites of DNA damage. *Nucleic Acids Res* **39**, 9224-9237
22. Islam, A., Chakraborty, A., Gambardella, S., Campopiano, R., Sarker, A. H., Boldogh, I., and Hazra, T. (2023) Functional analysis of a conserved site mutation in the DNA end processing enzyme PNKP leading to ataxia with oculomotor apraxia type 4 in humans. *J Biol Chem* **299**, 104714
23. Islam, A., Sakamoto, Y., Kosaka, K., Yoshitome, S., Sugimoto, I., Yamada, K., Shibuya, E., Vande Woude, G. F., and Hashimoto, E. (2005) The distinct stage-specific effects of 2-(p-amylcinnamoyl)amino-4-chlorobenzoic acid on the activation of MAP kinase and Cdc2 kinase in Xenopus oocyte maturation. *Cell Signal* **17**, 507-523
24. Gao, R., Chakraborty, A., Geater, C., Pradhan, S., Gordon, K. L., Snowden, J., Yuan, S., Dickey, A. S., Choudhary, S., Ashizawa, T., Ellerby, L. M., La Spada, A. R., Thompson, L. M., Hazra, T. K., and Sarkar, P. S. (2019) Mutant huntingtin impairs PNKP and ATXN3, disrupting DNA repair and transcription. *Elife* **8**
25. Peng, J., and Gygi, S. P. (2001) Proteomics: the move to mixtures. *J Mass Spectrom* **36**, 1083-1091
26. Shevchenko, A., Wilm, M., Vorm, O., and Mann, M. (1996) Mass spectrometric sequencing of proteins silver-stained polyacrylamide gels. *Anal Chem* **68**, 850-858
27. Eng, J. K., McCormack, A. L., and Yates, J. R. (1994) An approach to correlate tandem mass spectral data of peptides with amino acid sequences in a protein database. *J Am Soc Mass Spectrom* **5**, 976-989
28. Kalasova, I., Hailstone, R., Bublitz, J., Bogantes, J., Hofmann, W., Leal, A., Hanzlikova, H., and Caldecott, K. W. (2020) Pathological mutations in PNKP trigger defects in DNA single-strand break repair but not DNA double-strand break repair. *Nucleic Acids Res* **48**, 6672-6684

29. Reynolds, J. J., Walker, A. K., Gilmore, E. C., Walsh, C. A., and Caldecott, K. W. (2012) Impact of PNKP mutations associated with microcephaly, seizures and developmental delay on enzyme activity and DNA strand break repair. *Nucleic Acids Res* **40**, 6608-6619
30. Islam, A., Turner, E. L., Menzel, J., Malo, M. E., and Harkness, T. A. (2011) Antagonistic Gcn5-Hda1 interactions revealed by mutations to the Anaphase Promoting Complex in yeast. *Cell Div* **6**, 13
31. Parsons, J. L., Khoronenkova, S. V., Dianova, II, Ternette, N., Kessler, B. M., Datta, P. K., and Dianov, G. L. (2012) Phosphorylation of PNKP by ATM prevents its proteasomal degradation and enhances resistance to oxidative stress. *Nucleic Acids Res* **40**, 11404-11415
32. Tsukada, K., Shimada, M., Imamura, R., Saikawa, K., Ishiai, M., and Matsumoto, Y. (2021) The FHA domain of PNKP is essential for its recruitment to DNA damage sites and maintenance of genome stability. *Mutat Res* **822**, 111727
33. Mani, R. S., Mermershtain, I., Abdou, I., Fanta, M., Hendzel, M. J., Glover, J. N. M., and Weinfeld, M. (2019) Domain analysis of PNKP-XRCC1 interactions: Influence of genetic variants of XRCC1. *J Biol Chem* **294**, 520-530
34. Aceytuno, R. D., Piett, C. G., Havali-Shahriari, Z., Edwards, R. A., Rey, M., Ye, R., Javed, F., Fang, S., Mani, R., Weinfeld, M., Hammel, M., Tainer, J. A., Schriemer, D. C., Lees-Miller, S. P., and Glover, J. N. M. (2017) Structural and functional characterization of the PNKP-XRCC4-LigIV DNA repair complex. *Nucleic Acids Res* **45**, 6238-6251
35. Liu, Y., Wang, L., Han, R., Beier, U. H., Akimova, T., Bhatti, T., Xiao, H., Cole, P. A., Brindle, P. K., and Hancock, W. W. (2014) Two histone/protein acetyltransferases, CBP and p300, are indispensable for Foxp3+ T-regulatory cell development and function. *Mol Cell Biol* **34**, 3993-4007
36. Ogiwara, H., and Kohno, T. (2012) CBP and p300 histone acetyltransferases contribute to homologous recombination by transcriptionally activating the BRCA1 and RAD51 genes. *PLoS One* **7**, e52810
37. Dancy, B. M., and Cole, P. A. (2015) Protein lysine acetylation by p300/CBP. *Chem Rev* **115**, 2419-2452
38. Robson, C. N., Harris, A. L., and Hickson, I. D. (1989) Defective repair of DNA single- and double-strand breaks in the bleomycin- and X-ray-sensitive Chinese hamster ovary cell mutant, BLM-2. *Mutat Res* **217**, 93-100
39. Povirk, L. F., and Goldberg, I. H. (1987) A role of oxidative DNA sugar damage in mutagenesis by neocarzinostatin and bleomycin. *Biochimie* **69**, 815-823
40. Chen, J., Ghorai, M. K., Kenney, G., and Stubbe, J. (2008) Mechanistic studies on bleomycin-mediated DNA damage: multiple binding modes can result in double-stranded DNA cleavage. *Nucleic Acids Res* **36**, 3781-3790
41. Crossley, M. P., Song, C., Bocek, M. J., Choi, J. H., Kousorous, J., Sathirachinda, A., Lin, C., Brickner, J. R., Bai, G., Lans, H., Vermeulen, W., Abu-Remaileh, M., and Cimprich, K. A. (2023) R-loop-derived cytoplasmic RNA-DNA hybrids activate an immune response. *Nature* **613**, 187-194
42. Stork, C. T., Bocek, M., Crossley, M. P., Sollier, J., Sanz, L. A., Chedin, F., Swigut, T., and Cimprich, K. A. (2016) Co-transcriptional R-loops are the main cause of estrogen-induced DNA damage. *Elife* **5**

43. Ye, B. J., Kang, H. J., Lee-Kwon, W., Kwon, H. M., and Choi, S. Y. (2021) PARP1-mediated PARylation of TonEBP prevents R-loop-associated DNA damage. *DNA Repair (Amst)* **104**, 103132
44. Kemiha, S., Poli, J., Lin, Y. L., Lengronne, A., and Pasero, P. (2021) Toxic R-loops: Cause or consequence of replication stress? *DNA Repair (Amst)* **107**, 103199
45. Cong, S. Y., Pepers, B. A., Evert, B. O., Rubinsztein, D. C., Roos, R. A., van Ommen, G. J., and Dorsman, J. C. (2005) Mutant huntingtin represses CBP, but not p300, by binding and protein degradation. *Mol Cell Neurosci* **30**, 12-23
46. Giralt, A., Puigdellivol, M., Carreton, O., Paoletti, P., Valero, J., Parra-Damas, A., Saura, C. A., Alberch, J., and Gines, S. (2012) Long-term memory deficits in Huntington's disease are associated with reduced CBP histone acetylase activity. *Hum Mol Genet* **21**, 1203-1216
47. Jiang, H., Poirier, M. A., Liang, Y., Pei, Z., Weiskittel, C. E., Smith, W. W., DeFranco, D. B., and Ross, C. A. (2006) Depletion of CBP is directly linked with cellular toxicity caused by mutant huntingtin. *Neurobiol Dis* **23**, 543-551
48. Trettel, F., Rigamonti, D., Hilditch-Maguire, P., Wheeler, V. C., Sharp, A. H., Persichetti, F., Cattaneo, E., and MacDonald, M. E. (2000) Dominant phenotypes produced by the HD mutation in STHdh(Q111) striatal cells. *Hum Mol Genet* **9**, 2799-2809
49. Drazic, A., Myklebust, L. M., Ree, R., and Arnesen, T. (2016) The world of protein acetylation. *Biochim Biophys Acta* **1864**, 1372-1401
50. Shvedunova, M., and Akhtar, A. (2022) Modulation of cellular processes by histone and non-histone protein acetylation. *Nat Rev Mol Cell Biol* **23**, 329-349
51. Tahbaz, N., Subedi, S., and Weinfeld, M. (2012) Role of polynucleotide kinase/phosphatase in mitochondrial DNA repair. *Nucleic Acids Res* **40**, 3484-3495
52. Chappell, C., Hanakahi, L. A., Karimi-Busheri, F., Weinfeld, M., and West, S. C. (2002) Involvement of human polynucleotide kinase in double-strand break repair by non-homologous end joining. *EMBO J* **21**, 2827-2832
53. Sengupta, S., Yang, C., Hegde, M. L., Hegde, P. M., Mitra, J., Pandey, A., Dutta, A., Datarwala, A. T., Bhakat, K. K., and Mitra, S. (2018) Acetylation of oxidized base repair-initiating NEIL1 DNA glycosylase required for chromatin-bound repair complex formation in the human genome increases cellular resistance to oxidative stress. *DNA Repair (Amst)* **66-67**, 1-10
54. Bhakat, K. K., Hazra, T. K., and Mitra, S. (2004) Acetylation of the human DNA glycosylase NEIL2 and inhibition of its activity. *Nucleic Acids Res* **32**, 3033-3039
55. Bhakat, K. K., Izumi, T., Yang, S. H., Hazra, T. K., and Mitra, S. (2003) Role of acetylated human AP-endonuclease (APE1/Ref-1) in regulation of the parathyroid hormone gene. *EMBO J* **22**, 6299-6309
56. Bhakat, K. K., Mokkapati, S. K., Boldogh, I., Hazra, T. K., and Mitra, S. (2006) Acetylation of human 8-oxoguanine-DNA glycosylase by p300 and its role in 8-oxoguanine repair in vivo. *Mol Cell Biol* **26**, 1654-1665
57. Bhakat, K. K., Sengupta, S., and Mitra, S. (2020) Fine-tuning of DNA base excision/strand break repair via acetylation. *DNA Repair (Amst)* **93**, 102931
58. Akimaru, H., Chen, Y., Dai, P., Hou, D. X., Nonaka, M., Smolik, S. M., Armstrong, S., Goodman, R. H., and Ishii, S. (1997) Drosophila CBP is a co-activator of cubitus interruptus in hedgehog signalling. *Nature* **386**, 735-738

59. Shi, Y., and Mello, C. (1998) A CBP/p300 homolog specifies multiple differentiation pathways in Caenorhabditis elegans. *Genes Dev* **12**, 943-955
60. Janknecht, R. (2002) The versatile functions of the transcriptional coactivators p300 and CBP and their roles in disease. *Histol Histopathol* **17**, 657-668
61. Martire, S., Nguyen, J., Sundaresan, A., and Banaszynski, L. A. (2020) Differential contribution of p300 and CBP to regulatory element acetylation in mESCs. *BMC Mol Cell Biol* **21**, 55
62. Cazzalini, O., Sommatis, S., Tillhon, M., Dutto, I., Bachi, A., Rapp, A., Nardo, T., Scovassi, A. I., Necchi, D., Cardoso, M. C., Stivala, L. A., and Prosperi, E. (2014) CBP and p300 acetylate PCNA to link its degradation with nucleotide excision repair synthesis. *Nucleic Acids Res* **42**, 8433-8448
63. Dutto, I., Scalera, C., and Prosperi, E. (2018) CREBBP and p300 lysine acetyl transferases in the DNA damage response. *Cell Mol Life Sci* **75**, 1325-1338
64. Shen, J., Gilmore, E. C., Marshall, C. A., Haddadin, M., Reynolds, J. J., Eyaid, W., Bodell, A., Barry, B., Gleason, D., Allen, K., Ganesh, V. S., Chang, B. S., Grix, A., Hill, R. S., Topcu, M., Caldecott, K. W., Barkovich, A. J., and Walsh, C. A. (2010) Mutations in PNKP cause microcephaly, seizures and defects in DNA repair. *Nat Genet* **42**, 245-249
65. Bras, J., Alonso, I., Barbot, C., Costa, M. M., Darwent, L., Orme, T., Sequeiros, J., Hardy, J., Coutinho, P., and Guerreiro, R. (2015) Mutations in PNKP cause recessive ataxia with oculomotor apraxia type 4. *Am J Hum Genet* **96**, 474-479
66. Paucar, M., Malmgren, H., Taylor, M., Reynolds, J. J., Svenningsson, P., Press, R., and Nordgren, A. (2016) Expanding the ataxia with oculomotor apraxia type 4 phenotype. *Neurol Genet* **2**, e49
67. Poulton, C., Oegema, R., Heijsman, D., Hoogeboom, J., Schot, R., Stroink, H., Willemsen, M. A., Verheijen, F. W., van de Spek, P., Kremer, A., and Mancini, G. M. (2013) Progressive cerebellar atrophy and polyneuropathy: expanding the spectrum of PNKP mutations. *Neurogenetics* **14**, 43-51
68. Xia, W., Ci S., Li, M., et.al. (2019) Two-way crosstalk between BER and c-NHEJ repair pathway is mediated by Pol-β and Ku70. FASEB J. 33(11):11668-11681

Table 1: List of antibodies used in this study for protein of interest and internal controls

Primary antibodies	Source	Catalog#	Dilution
FLAG (M2)	Millipore Sigma	F 1804	1:500
Acetyl lysine K142 PNKP	Ez Biolabs	Custom-generated	1:200
Acetyl lysine K142 PNKP	Ez Biolabs	Custom-generated	1:200
PNKP	Bio-Bharati Life Sciences	BB AB0105	1:500
CBP	Santa Cruz Biotechnology	Sc-7300	1:1000
RNA polymerase II	Proteintech	920202	1:500
DNA polymerase eta	Cell Signaling Technology	13848	1:500
P300	Active Motif	61401	1:500
GAPDH	GeneTex	GTX100118	1:7000
HDAC2	GeneTex	GTX109642	1:500

XRCC1	GeneTex	GTX111712	1:500
XRCC4	GeneTex	GTX109632	1:500
DNA ligase III	In house (Ref-PMID: 26245904)		1:500
DNA ligase IV	GeneTex	GTX108820	1:500
Ku 70	GeneTex	GTX101820	1:500
Histone H2A.XS139ph (phosphoserine 139)	Cell Signaling Technology	6731	1:500
phosphor-53BP1	Cell Signaling Technology	2675	1:500
53BP1	Santa Cruz Biotechnology	Sc-517281	1:500
Neil2	In house (Ref-PMID: 26245904)		1:500
DNA polymerase □	Cell signaling Technology	13848S	1:500
RNA-DNA hybrid S9.6	Kerafast	ENH001	1:1000
dsDNA Ab	Abcam	ab215896	1:2000

Table 2: Primers used in the study

Primers	Gene	Nucleotide sequence 5′- 3′	Purpose
F1	PNKP (human)	GCGTATGCGGaggTCAAACCCCG-	For introducing K142R mutation
R1	PNKP (human)	TTCTTCGGCAGCTCAGCATC	For introducing K142R mutation
F2	PNKP (human)	CGGGCGCGGGaggCTGCCAGCCG	For introducing K226R mutation
R2	PNKP (human)	ATGCTCATCTGGTTGGTGAAGATCACCAGCTTGTAGCCCTCG	For introducing K226R mutation
F3	PNKP (human)	GCGTATGCGGcagTCAAACCCCG	For introducing K142Q mutation
R3	PNKP (human)	CGGGCGCGGGcagCTGCCAGCCG	For introducing K142Q mutation
F4	PNKP (human)	CGGGCGCGGGcagCTGCCAGCCG	For introducing K226Q mutation
R4	PNKP (human)	ATGCTCATCTGGTTGGTGAAGATCACCAGCTTGTAGCCC	For introducing K226Q mutation
F5	HPRT (human)	TGGGATTACACGTGTGAACCAACC	LA-qPCR
R5	HPRT (human)	GCTCTACCCTCTCCTCTACCGTCC	LA-qPCR
F6	HPRT (human)	TGCTCGAGATGTGATGAAGG	SA-PCR
R6	HPRT (human)	CTGCATTGTTTTGCCAGTGT	SA-PCR
F7	POLB (human)	CATGTCACCACTGGACTCTGCAC	LA-qPCR

R7	POLB (human)	CCTGGAGTAGGAACAAAAATTGCT	LA-qPCR
F8	POLB (human)	AGTGGGCTGGATGTAACCTG	SA-PCR
R8	POLB (human)	CCAGTAGATGTGCTGCCAGA	SA-PCR
F9	RNAPOLII (human)	AGGGGGTGTGTGAAGCAAAA	LA-qPCR
R9	RNAPOLII (human)	AGGGAGGCACATCTCTAGCA	LA-qPCR
F10	RNAPOLII (human)	CGCATTGACTTGCGTTTCCA	SA-PCR/ChIP-qPCR
R10	RNAPOLII (human)	CTGGGCAGCAACAGCCTTTA	SA-PCR/ChIP-qPCR
F11	NANOG (human)	CTCCGGAATGGTAGTCTGAGAAGAA	LA-qPCR
R11	NANOG (human)	ATTTAGGGCAGGCACAAGATGG	LA-qPCR
F12	NANOG (human)	ACCTACCTACCCCAGCCTTT	SA-PCR
R12	NANOG (human)	CATGCAGGACTGCAGAGATT	SA-PCR
F13	OCT4 (human)	TCTGTGGCCTCACCCTATGA	LA-qPCR
R13	OCT4 (human)	CAGACCTGTGGCAGGTATTGAA	LA-qPCR
F14	OCT4 (human)	GAAGGTATTCAGCCAAACGA	SA-PCR
R14	OCT4 (human)	GCACTGCAGGAACAAATTCT	SA-PCR
F15	MyH2 (human)	AAAGCCTGCCAAGCCCTAAA	LA-qPCR
R15	MyH2 (human)	TGGTCAGCATGGCAAGTGAA	LA-qPCR
F16	MyH2 (human)	GGCTCAAACTGCTGAAGGAGA	SA-PCR
R16	MyH2 (human)	TGGCACCAGGAGTTTTTGTCT	SA-PCR
F17	POLB (mouse)	TATCTCTCTTCCTCTTCACTTCTCCCCTGG	LA-qPCR
R17	POLB (mouse)	CGTGATGCCGCCGTTGAGGGTCTCCTG	LA-qPCR
F18	POLB (mouse)	TATGGACCCCCATGAGGAACA	SA-PCR
R18	POLB (mouse)	AACCGTCGGCTAAAGACGTG	SA-PCR
F19	TUBB (mouse)	GGTACAGGGGATGTGGTTGG	LA-qPCR
R19	TUBB (mouse)	GAGTCTCCTGCCTGTCCCTA	LA-qPCR
F20	TUBB (mouse)	AGCTCTTCACCAGGGTCTCT	SA-PCR
R20	TUBB (mouse)	TCTTTGTCTTCTGCCTCCAC	SA-PCR
F21	NeuroD (mouse)	CTCGCAGGTGCAATATGAATC	LA-qPCR
R21	NeuroD (mouse)	GCAACTGCATGGGAGTTTTCT	LA-qPCR
F22	NeuroD (mouse)	CTGCAAAGGTTTGTCCCAGC	SA-PCR
R22	NeuroD (mouse)	CTGGTGCAGTCAGTTAGGGG	SA-PCR
F23	MyH4 (mouse)	GACGTGGAACTGTTAGGCCA	LA-qPCR
R23	MyH4 (mouse)	AAGCCAGAGTCTTCAACCCG	LA-qPCR
F24	MyH4 (mouse)	GACGACCTTGAGCTGACACT	SA-PCR
R24	MyH4 (mouse)	TTGACTTTGTCCTCCTCTGC	SA-PCR
F25	MyH6 (mouse)	GACAAGGGGCATTGTAGCCT	LA-qPCR
R25	MyH6 (mouse)	TCTGCCTACCTTATGGGGCT	LA-qPCR
F26	MyH6 (mouse)	CCAGTGGAGGACCAAGTATG	SA-PCR
R26	MyH6 (mouse)	GTTCCTCTGCTTCTTGTCCA	SA-PCR

F27	MyoD (mouse)	ATAGACTTGACAGGCCCCGA	LA-qPCR
R27	MyoD (mouse)	GGACCGTTTCACCTGCATTG	LA-qPCR
F28	MyoD (mouse)	GCGGTTCAGGACCACTTATT	SA-PCR
R28	MyoD (mouse)	CCCGCTTGAGGAATAAACAT	SA-PCR
F29	GAPDH (human)	CATCACTGCCACCCAGAAGA	Internal control for gene expression
R29	GAPDH (human)	TTCTAGACGGCAGGTCAGGT	Internal control for gene expression
F 30	3'-UTR-PNKP (human)	GAGATCCCGTTCCGGCTATG	Expression of PNKP-3'-UTR
R30	3'-UTR PNKP (human)	CAGCGTTTATTGTGGAGGGG	Expression of PNKP-3'-UTR
F31	PNKP (human)	AATACGACTCACTATAGGGAG	Sequencing for confirmation of PNKP mutation(s) in pcDNA3
TV07 RPmix	NanoG (human)	RealTimePrimers.com	ChIP-qPCR
TV10 RPmix	Oct3/4 (human)	RealTimePrimers.com	ChIP-qPCR
TV11 RPmix	MyH2 (human)	RealTimePrimers.com	ChIP-qPCR
TV20 RPmix	β-Actin (human)	RealTimePrimers.com	ChIP-qPCR
HPRT1-In2-For	HPRT (human)	TGCCAGTATGGGTGGGAGAA	ChIP-qPCR
HPRT1-ln2-Rev	HPRT (human)	AGGGTAAAAACCCAGGCATGA	ChIP-qPCR

Figure 1

(A)

PPM	XCorr	ΔCorr	Peptide	Target amino acid
0.79	3.422	0.555	R.**K#**SNPGWENLEK.L	K142
0.92	2.091	0.694	R.G**K#**LPAEEFK.A	K226

(B)

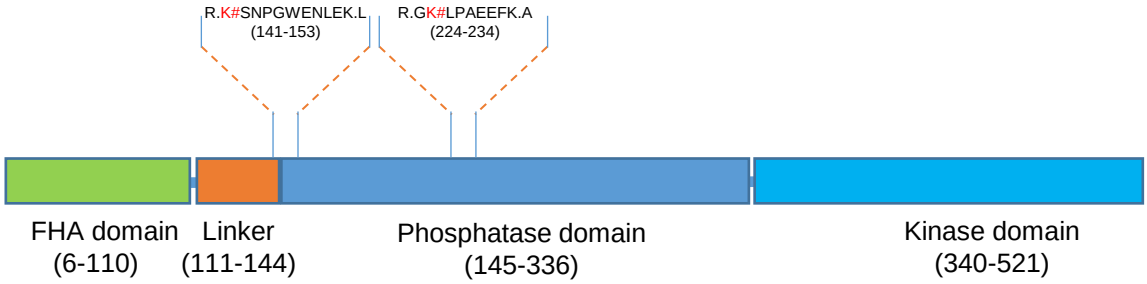

Figure 2

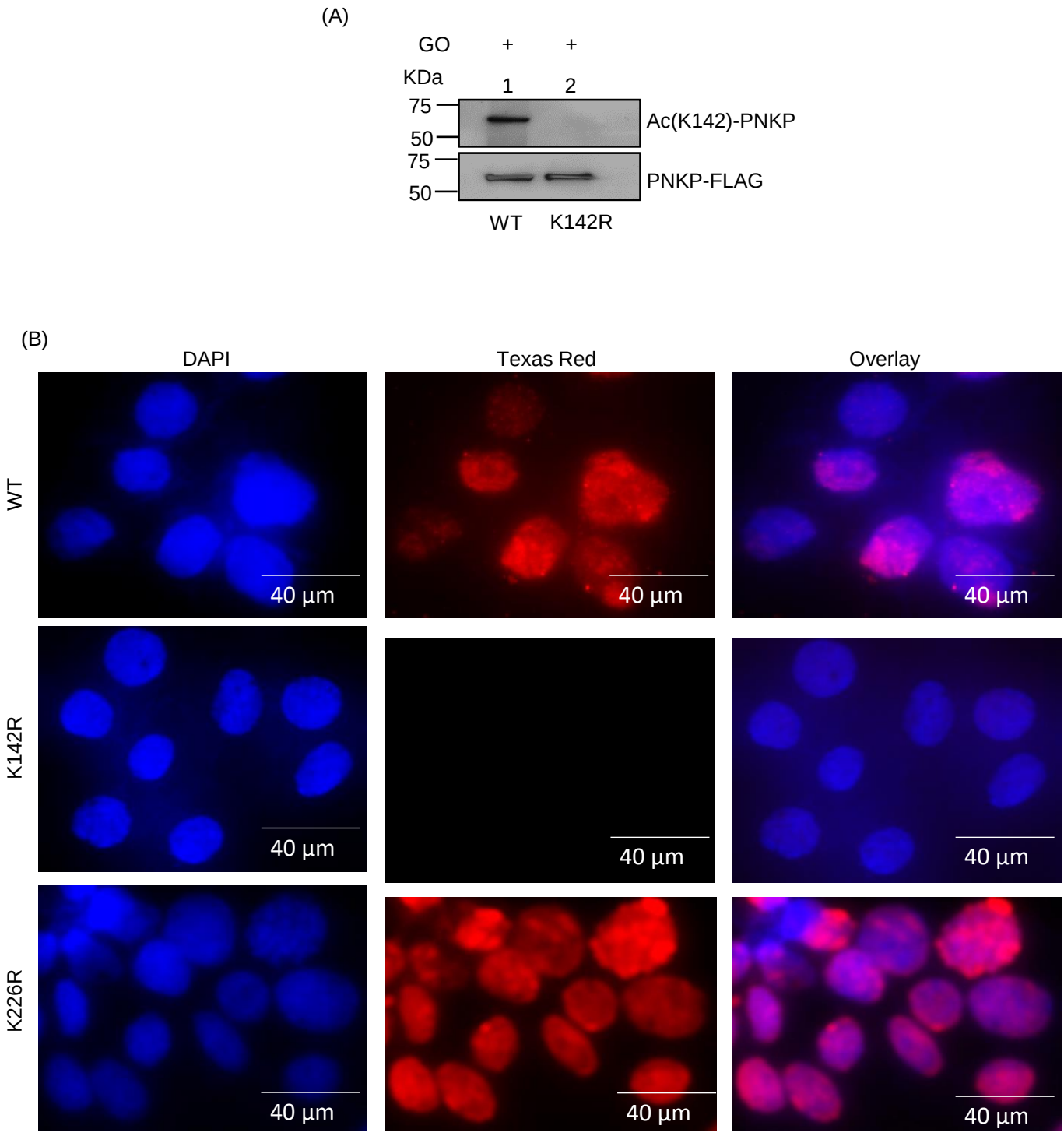
(A)
GO + +
KDa 1 2
75
50
75
50
Ac(K142)-PNKP
PNKP-FLAG
WT K142R
(B)
DAPI
Texas Red
Overlay
WT
K142R
K226R
40 µm

Figure 2 (contd)

(C)

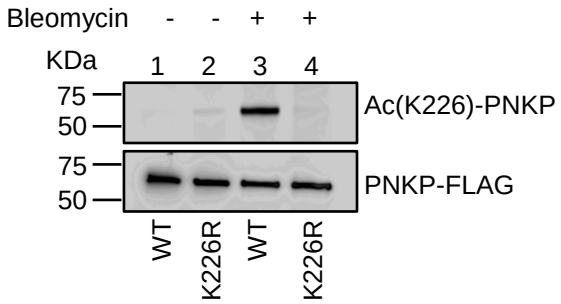

(D)

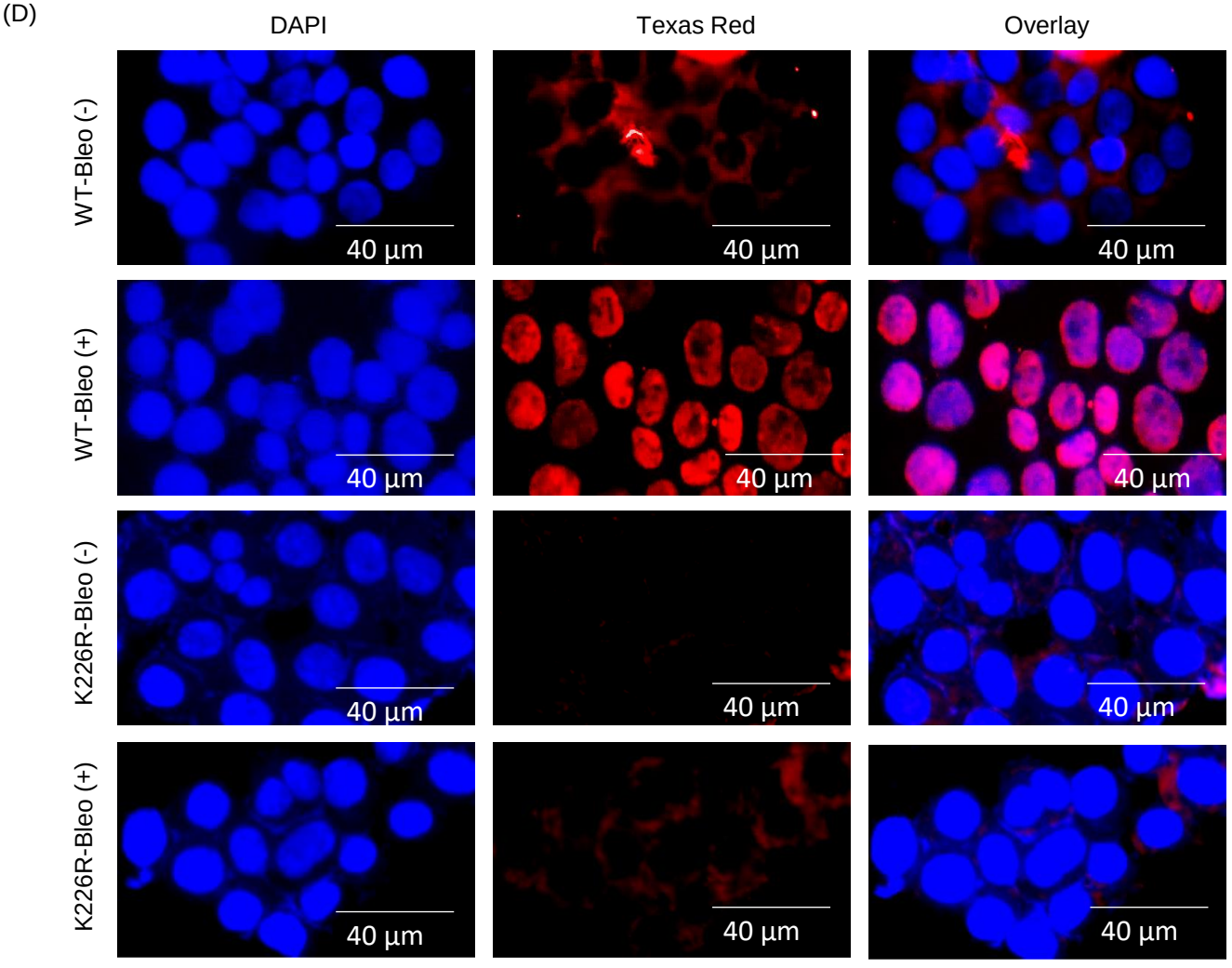

Figure 2 (contd)

(E)

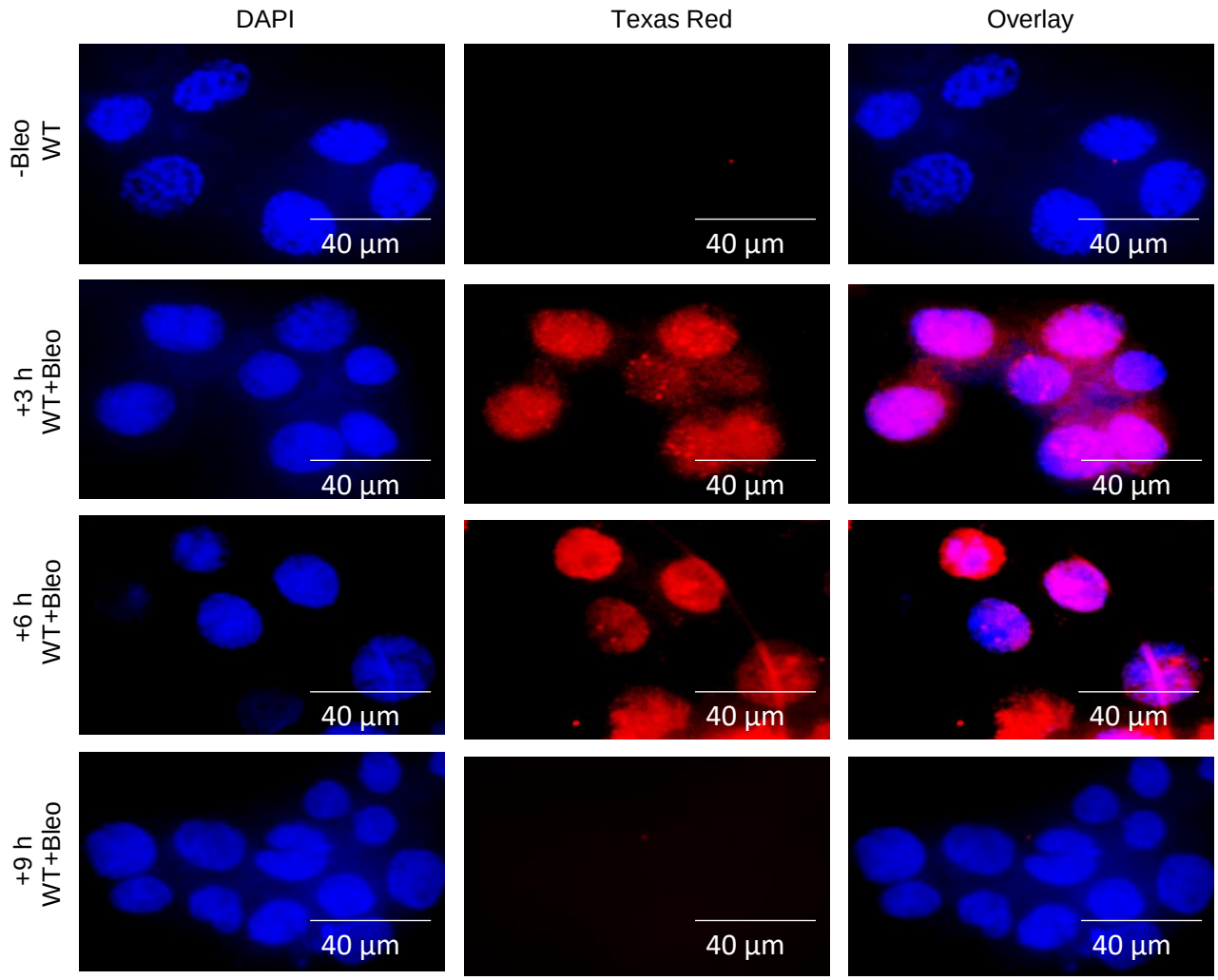

Figure 3

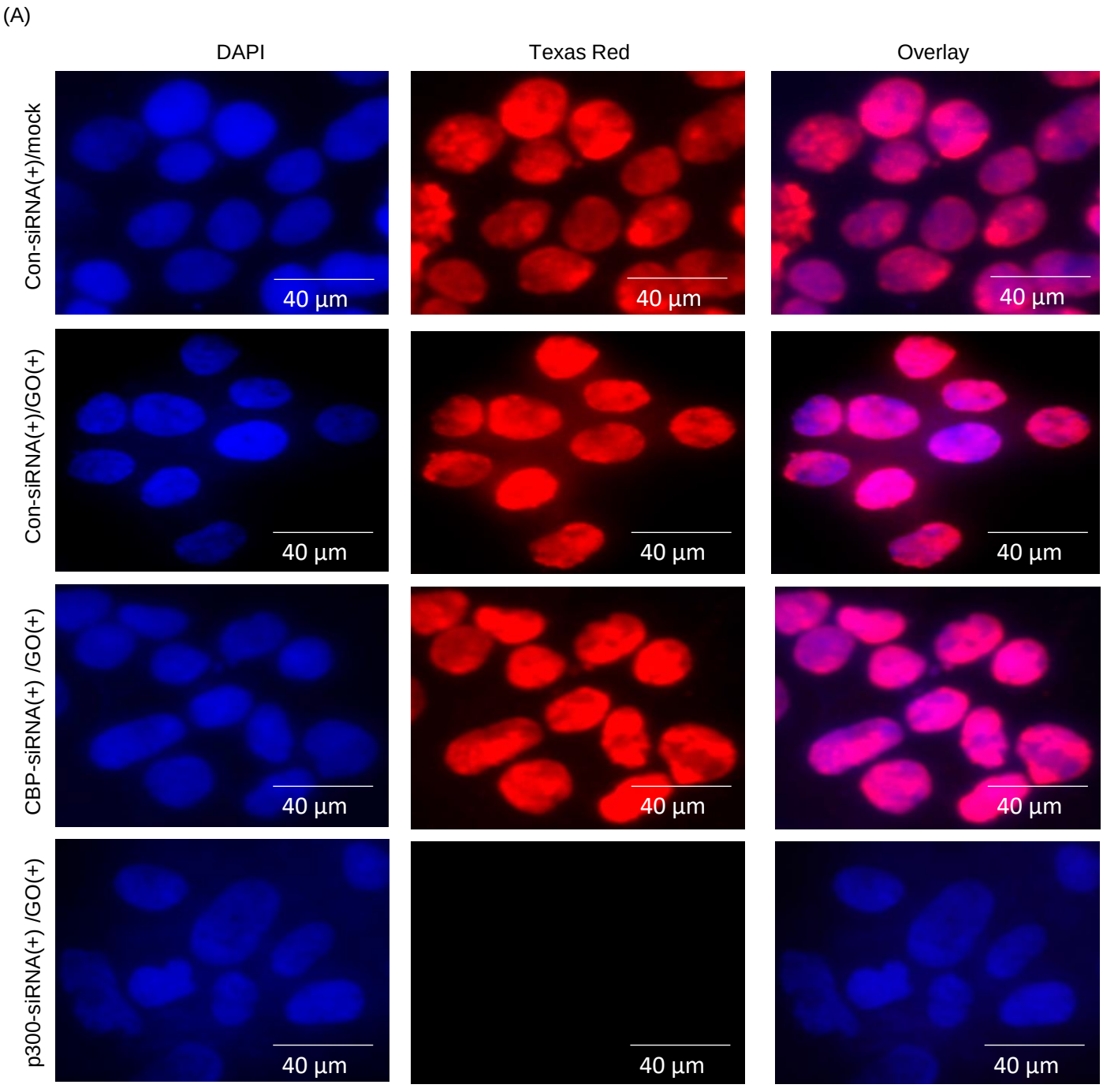
(A)
DAPI
Texas Red
Overlay
Con-siRNA(+)/mock
Con-siRNA(+)/GO(+)
CBP-siRNA(+) /GO(+)
p300-siRNA(+) /GO(+)
40 μm

Figure 3

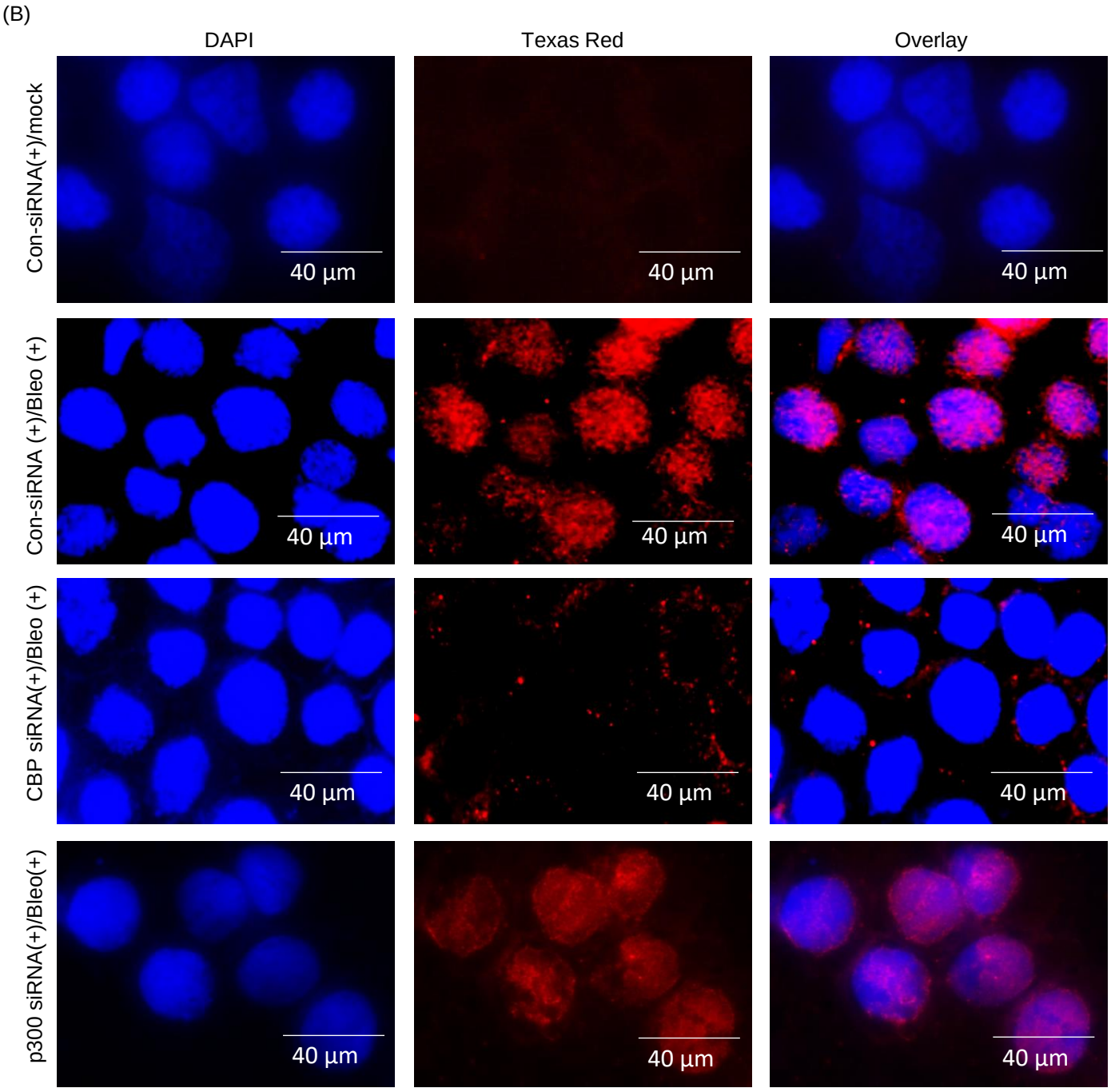
(B)
DAPI
Texas Red
Overlay
Con-siRNA(+)/mock
Con-siRNA (+)/Bleo (+)
CBP siRNA(+)/Bleo (+)
p300 siRNA(+)/Bleo(+)
40 µm

Figure 4

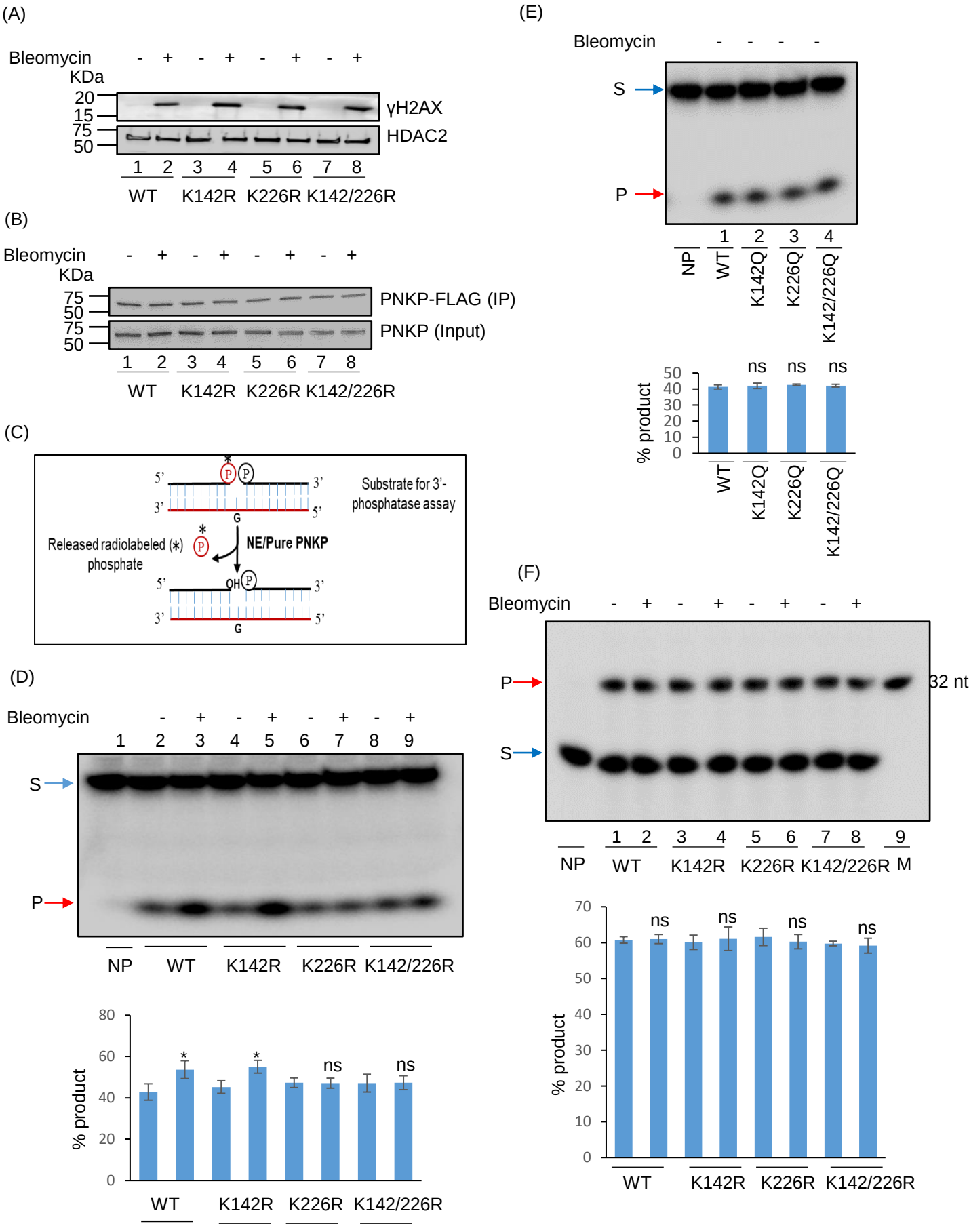
(A)
Bleomycin - + - + - + - +
KDa
20
15
75
50
γH2AX
HDAC2
1 2 3 4 5 6 7 8
WT K142R K226R K142/226R
(B)
Bleomycin - + - + - + - +
KDa
75
50
75
50
PNKP-FLAG (IP)
PNKP (Input)
1 2 3 4 5 6 7 8
WT K142R K226R K142/226R
(C)
5'
3'
P
Substrate for 3'-phosphatase assay
G
Released radiolabeled (*) phosphate
NE/Pure PNKP
OH
(D)
Bleomycin - + - + - + - +
1 2 3 4 5 6 7 8 9
S
P
NP WT K142R K226R K142/226R
% product
80
60
40
20
0
*
*
ns
ns
WT K142R K226R K142/226R
(E)
Bleomycin - - - -
S
P
NP 1 WT 2 K142Q 3 K226Q 4 K142/226Q
% product
50
40
30
20
10
0
ns ns ns
WT K142Q K226Q K142/226Q
(F)
Bleomycin - + - + - + - +
P
S
32 nt
1 2 3 4 5 6 7 8 9
NP WT K142R K226R K142/226R M
% product
70
60
50
40
30
20
10
0
ns ns ns ns
WT K142R K226R K142/226R

Figure 5

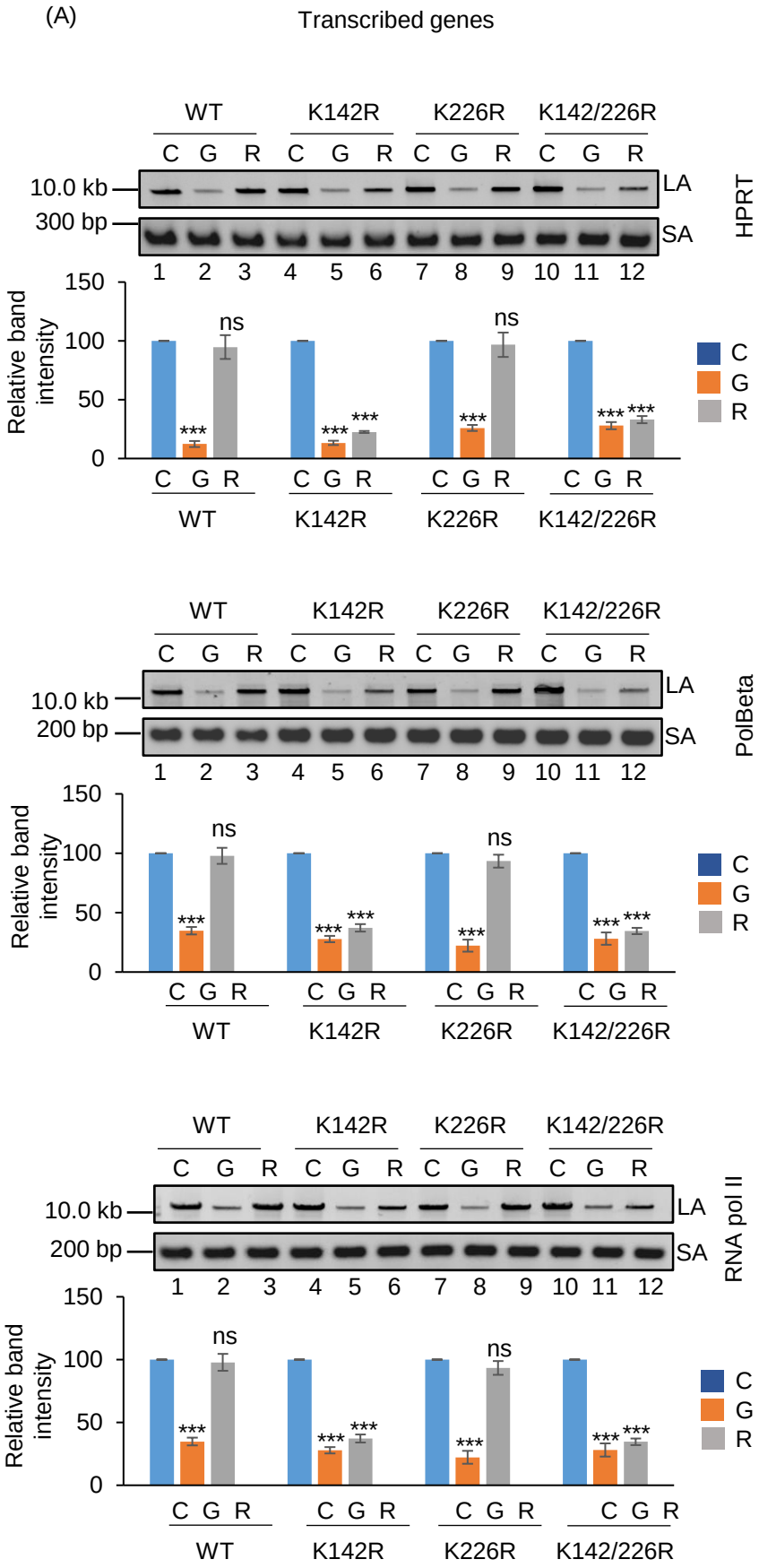
(A)
Transcribed genes
WT
K142R
K226R
K142/226R
C G R C G R C G R C G R
10.0 kb
300 bp
LA
SA
HPRT
1 2 3 4 5 6 7 8 9 10 11 12
Relative band intensity
150
100
50
0
ns
***
C
G
R
WT
K142R
K226R
K142/226R
10.0 kb
200 bp
PolBeta
RNA pol II

Figure 5 (contd)

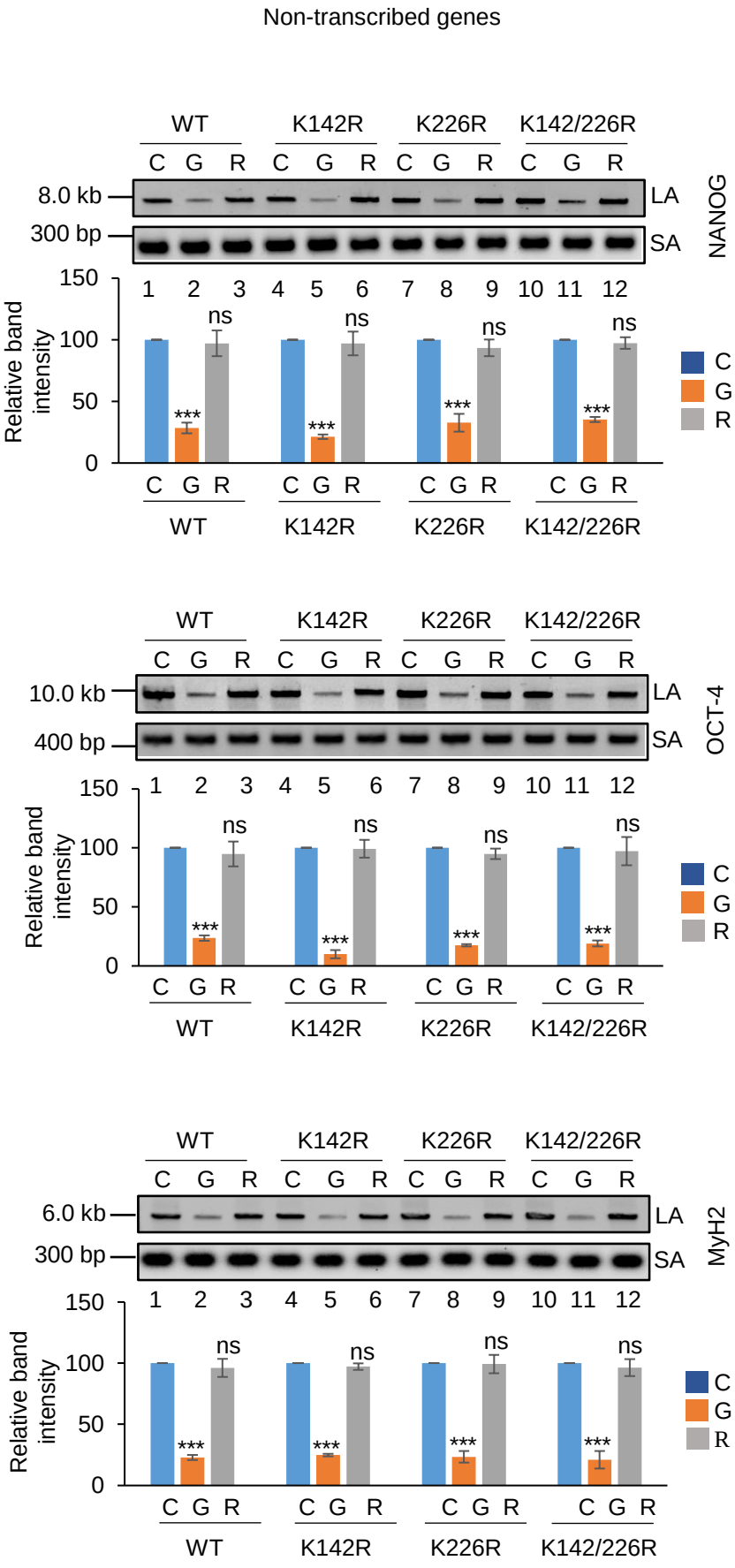

Figure 5 (contd)

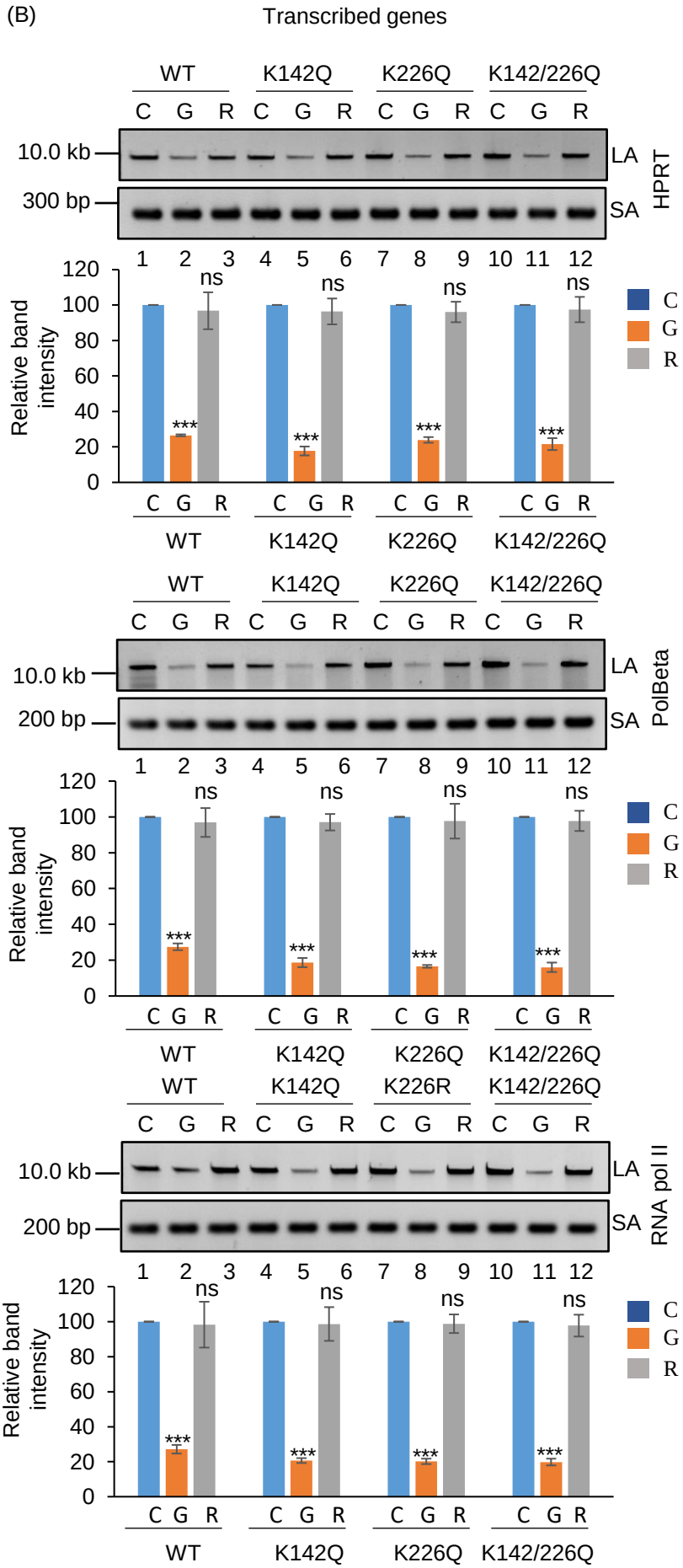

Figure 6

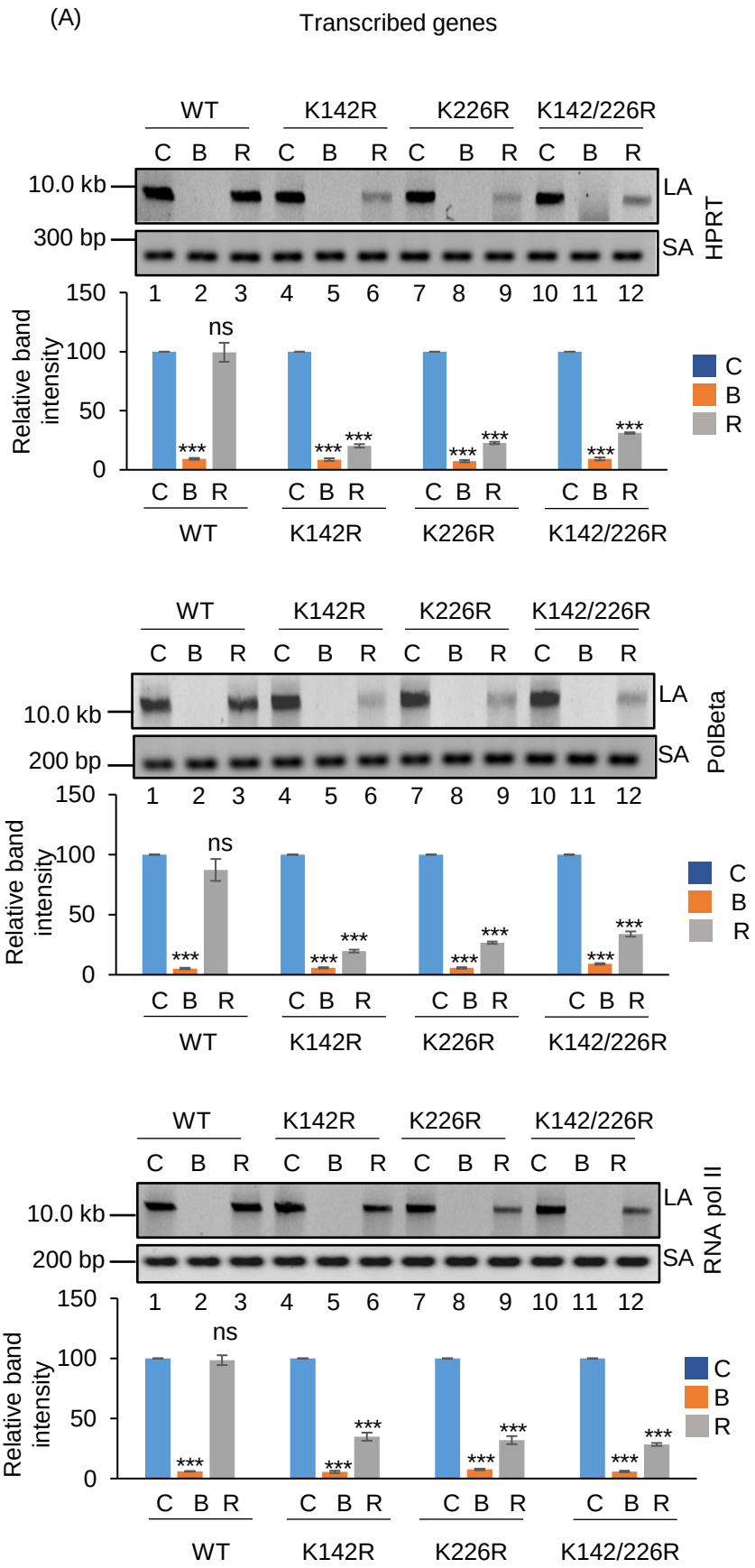
(A)
Transcribed genes
WT
K142R
K226R
K142/226R
C B R C B R C B R C B R
10.0 kb
300 bp
LA
SA
HPRT
1 2 3 4 5 6 7 8 9 10 11 12
Relative band intensity
150
100
50
0
ns
***
C
B
R
PolBeta
200 bp
RNA pol II

Figure 6 (contd)

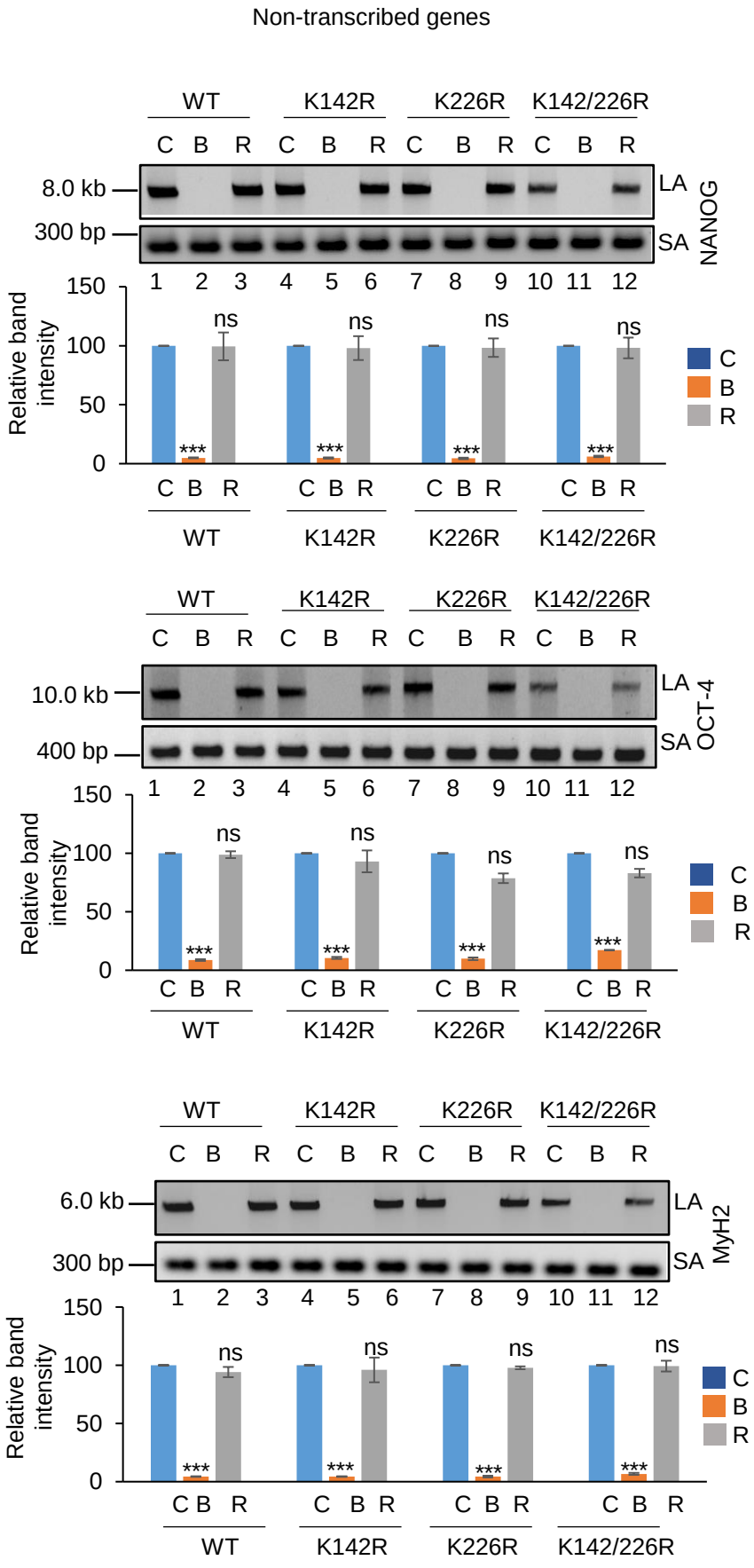

Figure 6 (contd)

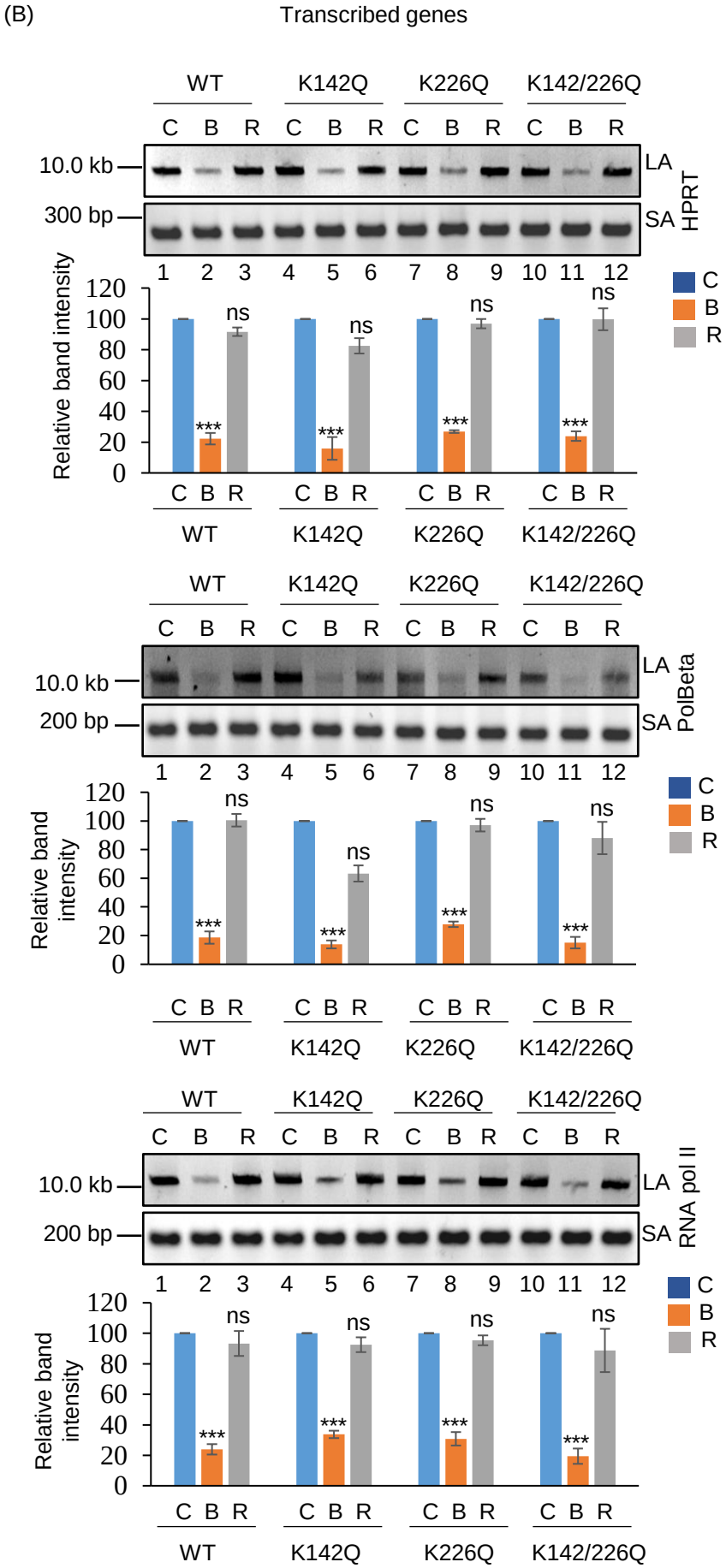

Figure 6 (contd)

(C)

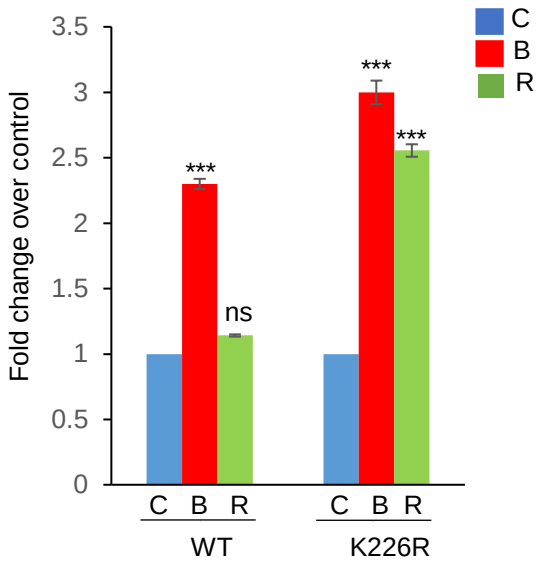

(D)

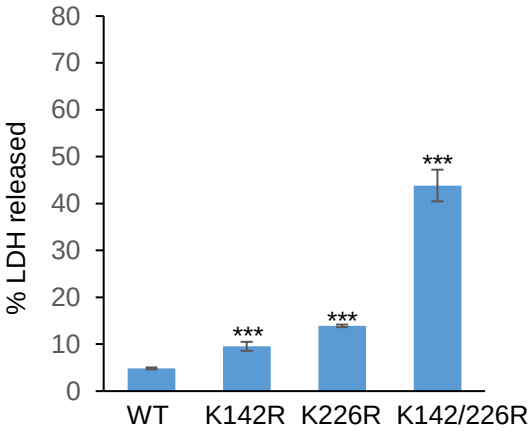

Figure 7

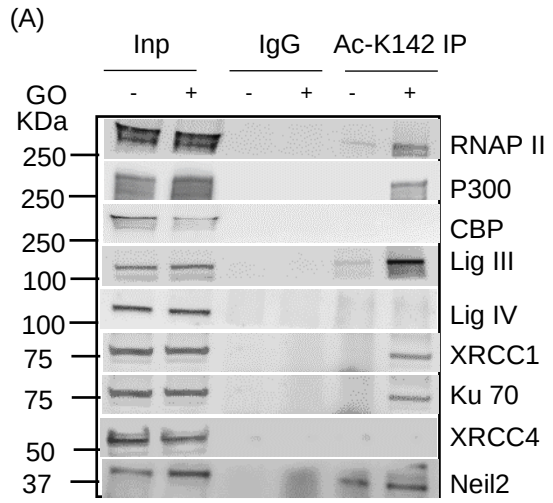
(A)
Inp
IgG
Ac-K142 IP
GO
- + - + - +
KDa
250
250
250
100
100
75
75
50
37
RNAP II
P300
CBP
Lig III
Lig IV
XRCC1
Ku 70
XRCC4
Neil2

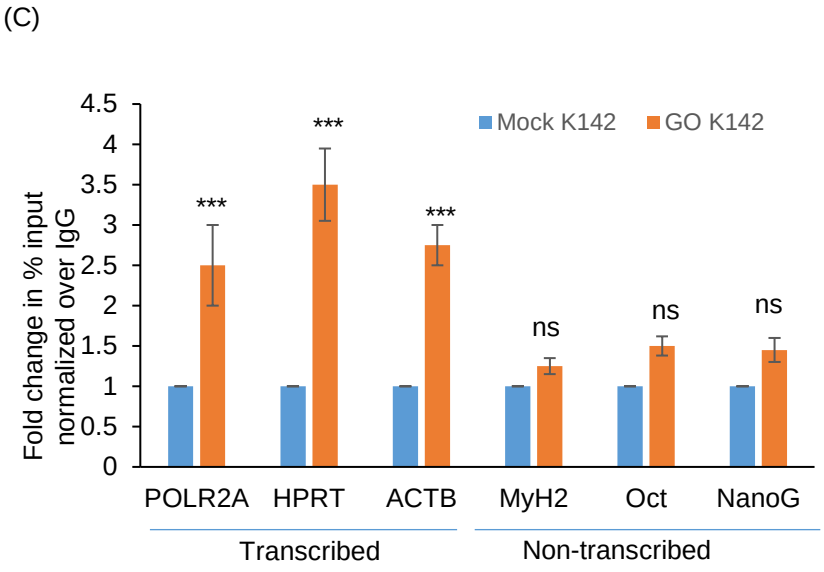
(C)
Mock K142
GO K142
Fold change in % input normalized over IgG
4.5
4
3.5
3
2.5
2
1.5
1
0.5
0
***
***
***
ns
ns
ns
POLR2A
HPRT
ACTB
MyH2
Oct
NanoG
Transcribed
Non-transcribed

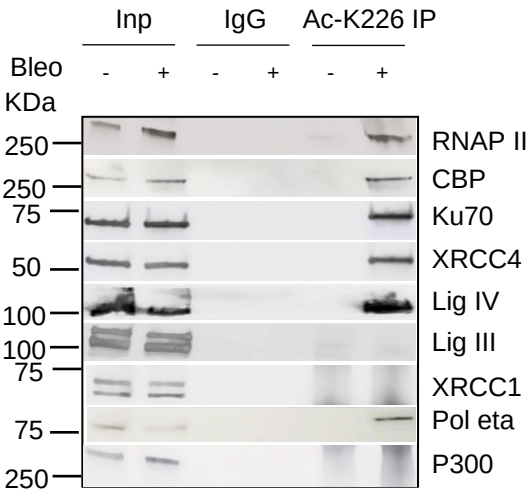
(B)
Inp
IgG
Ac-K226 IP
Bleo
- + - + - +
KDa
250
250
75
50
100
100
75
75
250
RNAP II
CBP
Ku70
XRCC4
Lig IV
Lig III
XRCC1
Pol eta
P300

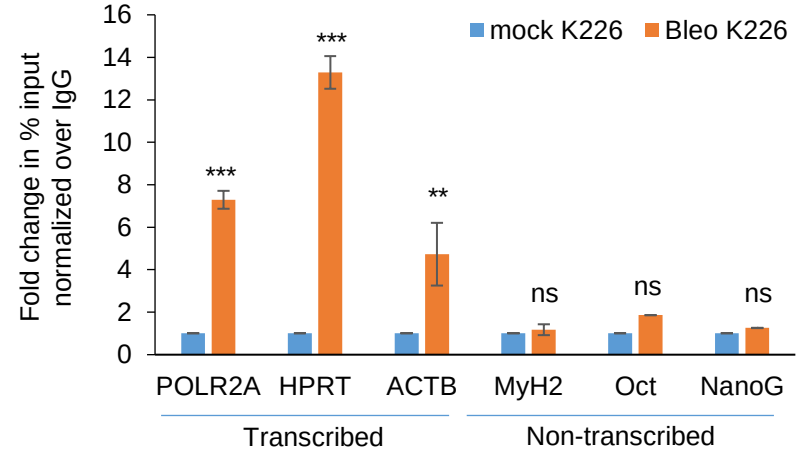
(D)
mock K226
Bleo K226
Fold change in % input normalized over IgG
16
14
12
10
8
6
4
2
0
***
***
**
ns
ns
ns
POLR2A
HPRT
ACTB
MyH2
Oct
NanoG
Transcribed
Non-transcribed

Figure 8

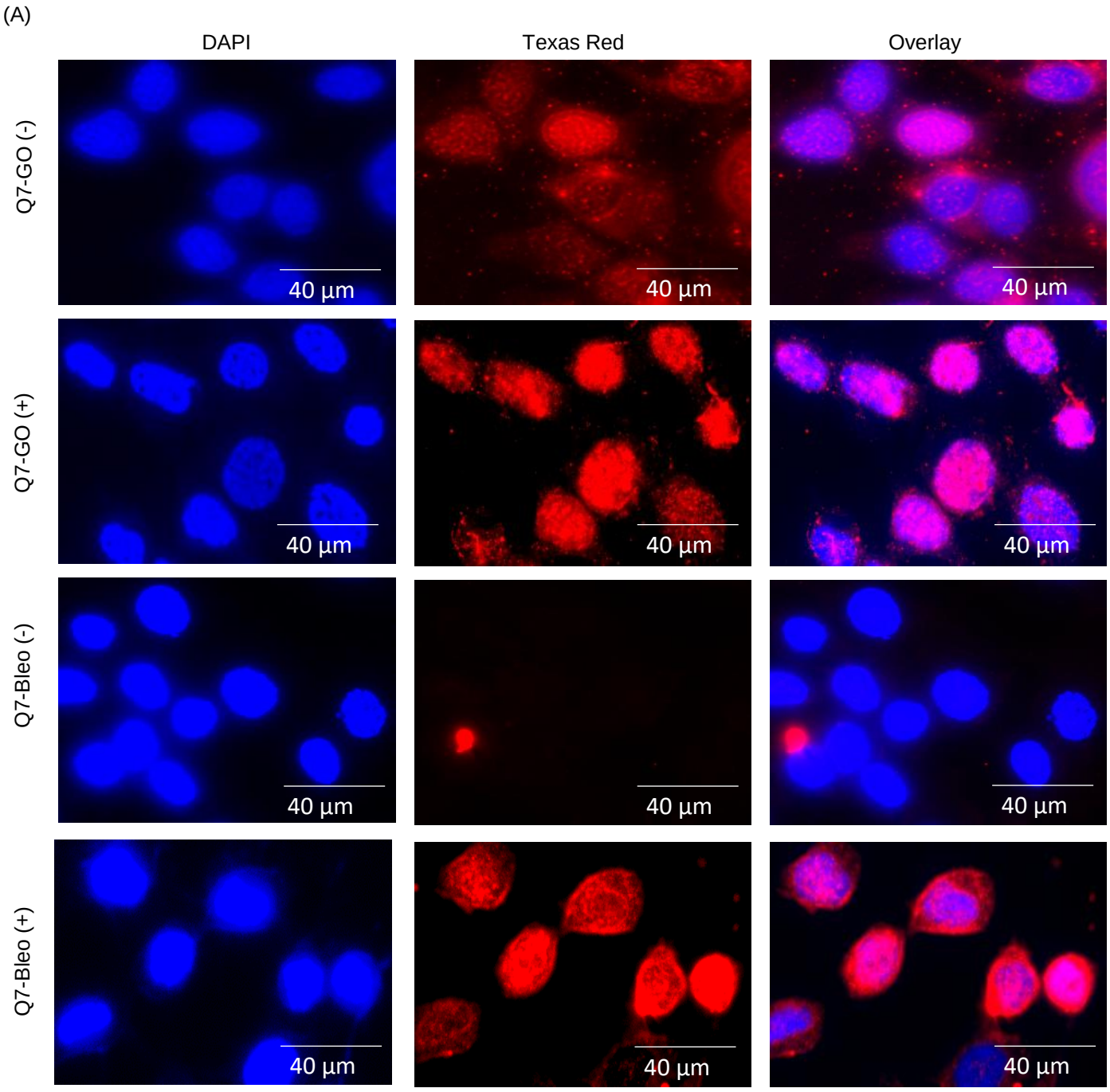

Figure 8 (contd)

(B)

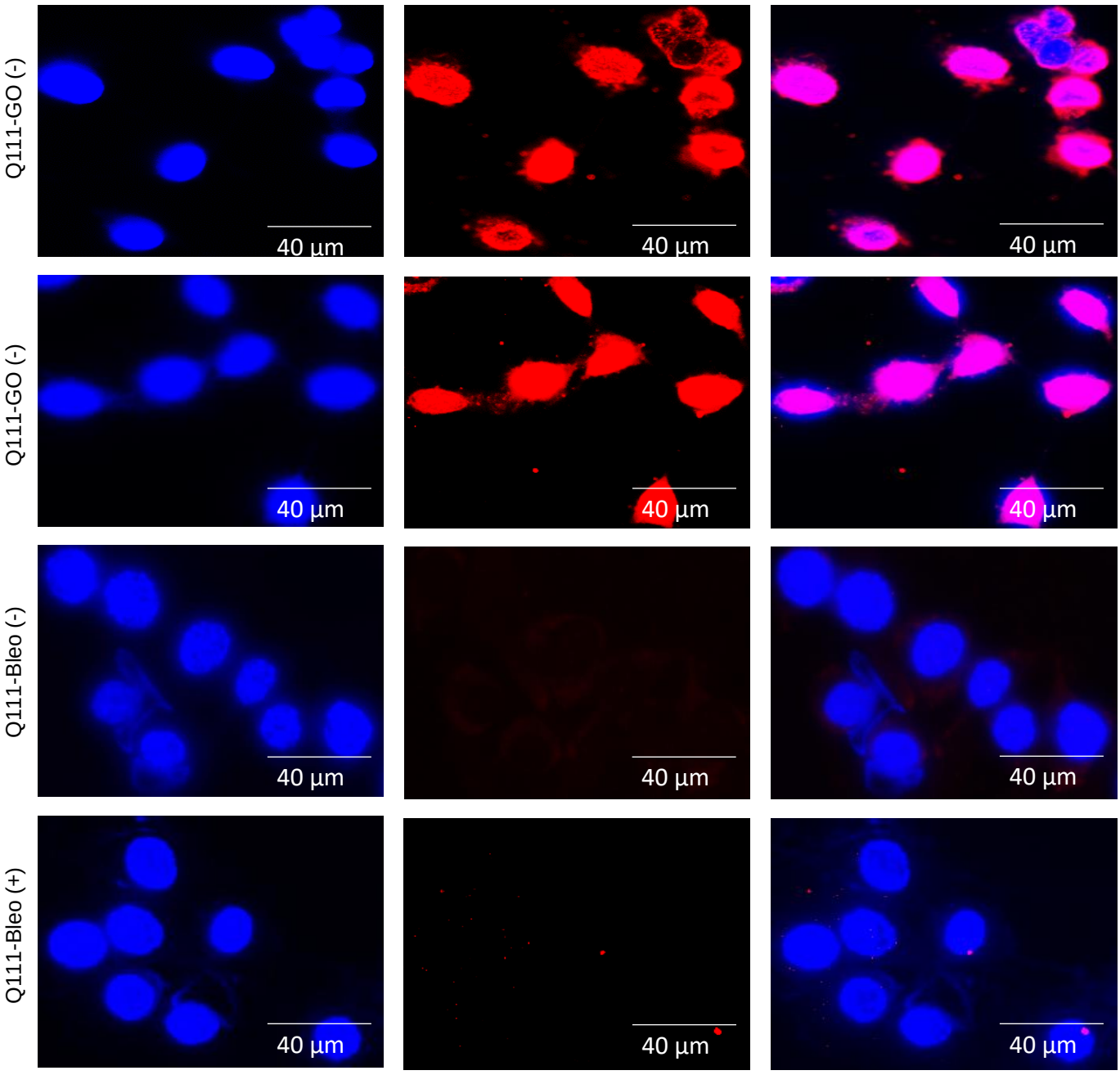

Figure 8 (contd)